Subduction and accumulation of lawsonite eclogite and garnet blueschist in eastern Australia

Tamblyn, Renée[1*], Hand, Martin[1], Kelsey, David[1,2], Anczkiewicz, Robert[3] and Och, David[4,5]

[1] Department of Earth Sciences, University of Adelaide, South Australia, 5005, Australia

[2] Geological Survey of Western Australia, East Perth, Western Australia, 6004, Australia

[3] Institute of Geological Sciences, Polish Academy of Sciences, Senacka 1, 31-002 Kraków, Poland

[4] School of Biological, Earth and Environmental Sciences, University of New South Wales, Kensington, New South Wales, 2052, Australia

[5] WSP Parsons Brinckerhoff, New South Wales, 2001, Australia

* renee.tamblyn@adelaide.edu.au

Abstract

Lawsonite eclogite and garnet blueschist occur as metre-scale blocks within serpentinite mélange in the southern New England Orogen in eastern Australia. These high-pressure fragments are the products of early Palaeozoic subduction of the palaeo-Pacific plate beneath East Gondwana. Lu–Hf, Sm–Nd and U–Pb geochronological data from Port Macquarie shows that eclogite mineral assemblages formed between ca. 500–470 Ma ago and became mixed together within a serpentinite-filled subduction channel. Age data and *P–T* modelling indicates lawsonite eclogite formed at around 2.7 GPa and 590 °C at ca. 490 Ma, whereas peak garnet in blueschist formed at around 2.0 GPa and 550 °C at ca. 470 Ma. The post-peak evolution of lawsonite eclogite was associated with preservation of pristine lawsonite-bearing assemblages and the formation of glaucophane. In contrast, the garnet blueschist was derived from a precursor garnet-omphacite assemblage. The geochronological data from these different aged high-pressure assemblages indicates the high-pressure rocks were formed during subduction on the margin of cratonic Australia during the Cambro-Ordovician. The rocks however now reside in the Devonian-Carboniferous southern New England Orogen, which forms the youngest and most outboard of the eastern Gondwanan Australian orogenic belts. Geodynamic modelling suggests that over the time scales that subduction products accumulated, the high-pressure rocks migrated large distances (ca. > 1000km) during slab retreat. Consequently, high-pressure rocks that are trapped in subduction channels may also migrate large distances prior to exhumation, potentially becoming incorporated into younger orogenic belts whose evolution is not directly related to the formation of the exhumed high-pressure rocks.

Keywords: eclogite; high-pressure; lawsonite; blueschist; accumulation; subduction

1. INTRODUCTION

High-pressure rocks which preserve eclogite and blueschist facies mineral assemblages are important recorders of subduction. Pressure–temperature–time (*P–T–t*) histories from high-pressure low-temperature rocks document the timing and physical conditions of subduction, as well as the potential durations that material resides within subduction channels prior to exhumation. These *P–T–t* histories provide important companionship to numerical models (e.g. Gerya, Stöckhert, & Perchuk, 2002; Stöckhert & Gerya, 2005; Peacock, 2003; Ruh, Pourhiet, Agard, Burov & Gerya, 2015) that seek to explain the burial and exhumation of material entrained within subduction channels.

High-pressure mélanges, which often contain eclogite and blueschist facies blocks encased within serpentinite and/or weakly metamorphosed sediments, are generally interpreted to reflect the subduction and subsequent mixing of lithologies within oceanic subduction channels (Bebout & Barton, 2002; Federico, Crispini, Scambelluri & Capponi, 2007). High-precision geochronology and well-constrained pressure-temperature estimates are beginning to reveal the complex histories contained within these mélanges (e.g. Wakabayashi & Dumitru, 2007; Krebs et al., 2008; Krebs, Schertl, Maresch, & Draper, 2011). A recurring finding is that subducted oceanic rocks now found mixed in mélange can record different *P–T–t* histories, implying they experienced different evolutions within the subduction channel before becoming exhumed together (Federico, Crispini, Scambelluri & Capponi, 2007; Krebs et al., 2008; Porteau et al., 2019). These samples can also record long-lived metamorphism within oceanic subduction channels, often coupled with generally slow exhumation rates (Guillot, Hattori, Agard, Schwartz, & Vidal, 2009;

Agard, Yamato, Jolivet, & Burov, 2009; Lázaro et al., 2009; Angiboust, Agard, Glodny, Omrani, & Oncken, 2016; Tamblyn et al., 2019). In order to preserve deeply buried, long-lived, refrigerated mineral assemblages, these oceanic-derived high-pressure rocks must reside for extended timescales within the subduction channel (Gerya, Stöckhert, & Perchuk, 2002). Numerical models show that subduction systems are unlikely to stay stationary for the apparent durations of cooling that have been recorded from high-pressure rocks (e.g. Baitsch-Ghiradello, Gerya, & Burg, 2014; Moresi, Betts, Miller, & Cayley, 2014). Logically, in order to continually exist in a low-temperature metamorphic environment, slowly exhuming material within the subduction channel must migrate with the trench. For the high-pressure exhumation durations implied by geochronology from the Caribbean (ca. 55 m.y.; Krebs et al., 2008; Lázaro et al., 2009) and Zagros (ca. 30 m.y.; Angiboust, Agard, Glodny, Omrani, & Oncken, 2016), trench migrations in excess of 1000 km appear realistic (Gerya, 2011; Baitsch-Ghiradello, Gerya, & Burg, 2014).

Arguably the thermobarometrically most sensitive high-pressure mineral assemblages that record low-temperature exhumation conditions are lawsonite-bearing eclogites, whose preservation appears to require cold, hydrous conditions be maintained during exhumation. Globally such assemblages are rare (Tsujimori & Ernst, 2014), despite the range of bulk compositions that should be able to stabilize lawsonite-garnet-omphacite bearing assemblages (Wei & Clarke, 2011). Well-preserved lawsonite strongly supports the concept that subducted oceanic material is exhumed via active subduction channels (Tsujimori & Ernst, 2014).

Lawsonite eclogite and garnet blueschist occur within serpentinite mélange in the Southern New England Orogen (SNEO) in eastern Australia. The SNEO is the youngest of three orogenic belts that formed on the margin of East Gondwana during the early to late Palaeozoic (Figure 1; Kemp, Hawkesworth, Collins, Gray, & Blevin, 2009; Glen, 2013; Rawlinson et al., 2014; Phillips, Offler, Rubatto, & Phillips, 2015). In this paper we present garnet Lu–Hf, Sm–Nd and zircon U–Pb data coupled with calculated phase equilibria forward models that constrain the timing of high-pressure metamorphism, as well as physical conditions of metamorphism. The results indicate early Palaeozoic lawsonite eclogite was subducted and tectonically mixed with younger high-pressure rocks within serpentinite-filled subduction channel.

2. GEOLOGICAL SETTING

The Tasmanides of eastern Australia consist of the Delamerian (515–490 Ma), Lachlan (484–340 Ma), and New England (305–230 Ma) orogens (Figure 1a; Kemp, Hawkesworth, Collins, Gray, & Blevin, 2009; Glen, 2013). The orogens are interpreted to have formed in response to subduction on the East Gondwanan margin. The SNEO is divided into three components: a Devonian–Carboniferous volcanic arc in the west, a forearc basin, and an accretionary wedge to the east (Jenkins, Landenberger, & Collins, 2002). In the SNEO, the Tamworth Belt represents a Late Devonian–Carboniferous forearc basin and the Tablelands Complex represents a Silurian–Carboniferous accretionary complex. These are separated by the serpentinite-bearing Peel Manning Fault System (PMFS; Figure 1b; Aitchison & Ireland, 1995; Jenkins, Landenberger, & Collins, 2002).

Rare, high-pressure low-temperature metamorphic blocks occur in the SNEO within serpentinite at Attunga, Gleneden, Glenrock, Pigna Barney and Port Macquarie (Figure 1b). Eclogite facies metamorphism at Attunga has been constrained to the mid to late

Cambrian by zircon U–Pb geochronology (Phillips, Offler, Rubatto, & Phillips, 2015; Manton, Buckman, Nutman, & Bennet, 2017). Cooling or peak blueschist metamorphism has been constrained by $^{40}Ar/^{39}Ar$ and K–Ar geochronology to the Ordovician–Silurian (Fukui, Watanabe, Itaya, & Leitch, 1995; Sano, Offler, Hyodo, & Watanabe, 2004; Och, Leitch, Caprarelli, & Watanabe, 2003; Phillips, 2010; Phillips & Offler, 2011; Phillips, Offler, Rubatto, & Phillips, 2015).

Within the SNEO, the Port Macquarie mélange is unique in the abundance and lithological range of the high-pressure metamorphic blocks (Barron, Scheibner & Slanksy 1976, Och, Leitch, Caprarelli & Watanabe, 2003; Och, 2007; and Och, Leitch & Caprarelli, 2007). The mélange consists of two lenses of chlorite-actinolite schist separated by a domain of serpentinite (Figure 1c). The metamorphic blocks consist of variably foliated high-pressure rocks mostly of probable mafic igneous origin. Blocks comprise blueschist facies conglomerate, marble and other sedimentary rocks (Figure 2a). The high-pressure metamorphic blocks make up about 20% of the mélange. Rounded eclogite blocks range up to 2 m across and are characterised by abundant euhedral garnet up to 1 cm, but more commonly 2–5 mm, set in either an omphacite rich matrix or together with euhedral lawsonite porphyrobasts, set in a phengite rich matrix (Figure 2b). In some instances, blocks consist of essentially monomineralic unfoliated omphacite, with less abundant lawsonite (Och et al., 2003). In several of the eclogite blocks, the eclogite assemblages have been partially replaced by glaucophane schist. Blueschist blocks range up to at least 6 m in their longest dimension, and usually have a strong foliation that ranges from planar to intensely folded. Some of the blueschist was clearly derived from a conglomerate protolith, and contains highly deformed prolate clasts up to 20 cm long of probable volcanic origin. There are two varieties of garnet-bearing blueschist. One is intensely foliated with porphyroblasts of garnet and lawsonite enclosed by a glaucophane dominated matrix. The other variety is weakly foliated with garnet porphyroblasts commonly occurring in clump like aggregates (Figure 2c).

Ordovician (ca. 470 Ma) K–Ar ages have been obtained from late-stage phengite in blueschist, which have been interpreted to provide a lower age limit on the timing of the high-pressure metamorphism (Fukui, Watanabe, Itaya, & Leitch, 1995). In contrast, Nutman et al. (2013) dated zircons interpreted to be detrital in origin within eclogite, to provide an apparent maximum possible age for eclogite metamorphism of 251±6 Ma and attributed the older K–Ar ages to excess argon. Och et al. (2003) obtained *P–T* conditions for the eclogite assemblages of ~1.8 GPa and 560 °C using conventional thermobarometry and rudimentary *P–T* grids, and lower-temperature conditions of ~360–450 °C for the blueschist facies conditions. Conversely, Nutman et al. (2013) suggested the eclogite and blueschist experienced the same *P–T* history, with maximum conditions less than 450 °C and 1.0 GPa, arguing the blueschist and eclogite assemblages reflect variations in bulk composition.

3. SAMPLES

The samples used in this study come from: (1) a 2 by 1.5 m block of garnet-lawsonite-omphacite-phengite at the southern end of the Port Macquarie mélange that contains domains of retrograde blueschist that were avoided during sampling (Figure 2b) and (2) a weakly foliated garnet-bearing blueschist from a 2 by 1 metre block, approximately 3 meters away from the garnet-lawsonite-omphacite-phengite block (Figure 2c; 31º26’14.02” S, 152º55’31.54” E). Both blocks have broken free of the chlorite-actinolite matrix (Figure 1c, 2a), and their current proximity may simply reflect the vigorous wave action on the beach. In both samples, proportions of minerals were determined by mapping with a scanning electron microscope (SEM) with mineral liberation analysis (MLA) software.

RB11: lawsonite eclogite

The abundant phengite in sample RB11 means it mineralogically does not represent a true eclogite *sensu stricto*, rather it is an eclogite-facies rock. For simplicity, the term lawsonite eclogite will be used, to encompass the thermobarometrically important mineralogy and conditions reached by the sample. The sample contains porphyroblastic euhedral lawsonite (up to 3 mm), garnet (up to 7 mm) and omphacite (up to 1 mm) in a phengite-dominated matrix (Figure 3a,b). The phengite (48% of the rock; determined by mineral liberation analysis (MLA) mapping) contains minor but well distributed fine-grained titanite trails that parallel the phengite foliation. Garnet comprises 20% of the rock and contains inclusions of lawsonite, titanite, omphacite, chlorite, glaucophane, phengite, epidote, quartz, stilpnomelane and zircon (Figure 3c). Lawsonite comprises 7% of the assemblage and contains inclusions of titanite, glaucophane, garnet, epidote and phengite (Figure 3d). In both garnet and lawsonite, fine-grained titanite defines sigmodal inclusion trails that are sometimes truncated within near rim locations within the porphyroblasts by inclusions trails of a younger titanite defined foliation. Chlorite and stilpnomelane inclusions are predominantly in the garnet cores (Figure 3c). Garnet is locally replaced by chlorite (Figure 3b,c). Omphacite (5% of the rock) forms small porphyroblasts with garnet and lawsonite, which are partially replaced by chlorite and glaucophane (Figure 3a,b). Elsewhere, glaucophane occurs with chlorite within micro-boudin necks in deformed aggregates of garnet-omphacite-lawsonite (Figure 3b). Retrograde glaucophane and chlorite comprise 9% each of the rock.

RB12: garnet blueschist

RB12 contains garnet porphyroblasts up to 6mm in diameter, which are transected by aragonite-quartz veins and partially pseudomorphed by chlorite (Figure 2c, Figure 3e). Aragonite was optically identified as carbonate with a low 2V biaxial negative interference figure. The relic garnet now comprises 5% of the assemblage. However, the original outlines of garnet are still easily discernible, and prior to its partial replacement, it comprised 13% of the rock. Garnet contains inclusions of omphacite, with lesser amounts of glaucophane, quartz, rutile and phengite (Figure 3f). Omphacite is abundant in some garnets, forming a myriad of small irregular grains that occur throughout the garnet (Figure 3f). The rock matrix consists of glaucophane (80%), phengite (6%) and quartz (3%), lawsonite (<1 %) and titanite that mantles rutile. The abundance of glaucophane in the matrix and its existence as inclusions within garnet suggests it was present throughout the development of peak to retrograde conditions. There is no omphacite in the matrix, but its presence as inclusions in garnet suggests that it was present prior to retrograde conditions, possibly at eclogite facies.

4. ANALYTICAL METHODS

4.1 Electron Probe Micro Analyses and X-Ray mapping

Spot analyses were obtained using a Cameca SX-5 WDS electron microprobe with a beam current of 20 nA and an accelerating voltage of 15 kV, with an andradite crystal analysed for calibration. Zr maps used a 200 nA beam current and an accelerating voltage of 15 kV, and Zr was mapped using Wavelength Dispersive Spectrometers (WDS).

4.2 LA–ICP–MS mapping

Rare earth elements were mapped in garnet and lawsonite to aid in the interpretation of Sm–Nd and Lu–Hf ages. This was done using an ASI m50 LA–ICP–MS with an Agilent 7900 MS. Mapping targeted Lu and Sm to determine elemental concentrations. The data was processed in Iolite (Paton, Hellstrom, Paul, Woodhead & Hergt, 2011), using Ca as the index element. Quantitative maps were processed using the Matlab script XMapTools (Lanari et al., 2014).

4.3 Lu–Hf and Sm–Nd geochronology

Garnet and lawsonite were separated using crushing, magnetic separations, heavy liquid procedures and hand-picking to obtain pure (>99%) mineral samples. Whole rock samples were obtained by pulverising a representative part of the rock. Lu–Hf and Sm–Nd analyses were collected at the Kraków Research Centre, Institute of Geological Sciences, Polish Academy of Sciences. Analyses followed the methods of Anczkiewicz and Thirlwall (2003) with modifications for the Lu–Hf method from Anczkiewicz, Platt, Thirlwall, & Wakabayashi (2004). JMC475 measured over the course of analyses yielded $^{176}Hf/^{177}Hf = 0.282161 \pm 8$, and $^{143}Nd/^{144}Nd = 0.51209697 \pm 8$ for JNd-1 standard over the course of analyses. For age calculations internal errors were used. Isochron plots were done using Isoplot (Ludwig, 2003). All uncertainties are reported as 2 sigma.

4.4 U–Pb geochronology

Zircon geochronology was undertaken in-situ on zircons from the lawsonite eclogite. Zircons from the eclogite were identified and imaged within polished rock blocks using a Quanta 600 Scanning Electron Microscope. Attempts to image zircons using cathodoluminescence (FEI, Quanta 600) were unsuccessful. The zircons showed a bland low intensity response that likely resulted from their fine-grain size (< 15 μm) and hosting within silicate minerals. Isotopic compositions of ^{204}Pb, ^{206}Pb, ^{207}Pb, ^{208}U, ^{232}Th and ^{238}U were measured using a New Wave 213 nm Nd–YAG laser, coupled with an Agilent 7500cs/7500s ICP–MS. Given the small size of the in-situ zircons a spot size of 10 μm was used. Due to the small spot size and resulting low counts during acquisition, trace element compositions of the zircons were not collected. A frequency of 5 Hz was used with an acquisition time of 60 seconds, including 30 seconds of background measurement and 30 seconds of ablation. Data analyses and correction for mass bias and elemental fractionation utilizing the program Glitter (Griffin, Belousova, Shee, Pearson & O'Reilly, 2004), and the primary zircon standard GJ. Instrument drift was accounted for using a linear correction and standard bracketing every 5 zircon analyses. Age calculations were done using Isoplot (Ludwig, 2003). All uncertainties on U–Pb ages are reported as 1 sigma. Over the course of the analyses, the primary standard GJ returned a $^{206}Pb/^{238}U$ weighted mean age of 596.9±4.3 Ma (n = 48, MSWD = 1.8) and a $^{207}Pb/^{235}U$ weighted mean age of 596.7±6.4 Ma (n = 48, MSWD = 0.88). The secondary standard Plesovice returned a $^{206}Pb/^{238}U$ weighted mean age of 329.8±5.3 Ma (n = 12, MSWD – 1.9) and a $^{207}Pb/^{235}U$ weighted mean age of 340.1±7.7 Ma (n = 12, MSWD = 0.54).

4.5 Phase equilibria forward modelling

Metamorphic geochemistry was determined for the eclogite and blueschist by combining determined modal proportions of each mineral with their measured composition (Table 1; Supplementary Table 1; 2). This was done as both samples contain retrograde carbonate and quartz veins that may have been derived from beyond the effective metamorphic bulk composition and would have been incorporated into any XRF bulk rock analysis. Thin sections were mapped using a scanning electron microscope

(SEM) with mineral liberation analysis software (MLA) to identify and calculate the modal proportions of metamorphic minerals. The mineral volumes were then converted to weight percent estimates by applying densities based on their average compositions. These modal proportions where then integrated to create a bulk composition for modelling.

Phase equilibria modelling was undertaken using THERMOCALC (Powell & Holland, 1988; Holland & Powell, 2011) employing the internally-consistent thermodynamic dataset ‘ds5’ (filename tc-ds55.txt; November 2003 updated version of the Holland & Powell, 1998 data set) and activity–composition models (Powell & Holland, 1988; Holland & Powell, 2003; White, Powell, & Holland 2007; Green, Holland, & Powell, 2007; Holland & Powell, 2011; Diener & Powell, 2012). The latest thermodynamic dataset ‘ds62’ (Green et al., 2016) was not used, as calculations could not solve for equilibria with multiple amphibole or clinopyroxene end-members.

Mn was incorporated in the whole rock bulk compositional calculations to predict the stability of garnet on the prograde path. Further, calculations for the lawsonite eclogite in the MnNCKFMASHTO system predicted the stable coexistence of rutile–garnet–lawsonite–omphacite–phengite ± glaucophane ± chlorite in the modelled bulk composition, whereas the rock contains the assemblage titanite–garnet–lawsonite–omphacite–phengite, with retrograde glaucophane and chlorite. The presence of titanite rather than rutile may reflect the role of Fe^{3+} and Al substitution as well as the presence of a H_2O-rich fluid , which expands the stability of titanite up pressure (Enami, Suzuki, Liou, & Bird, 1993; Carswell, Wilson, & Zhai, 1996; Brovarone, Groppo, Hetényi, Compagnoni, & Malavieille, 2001; Castelli & Rubatto, 2002). In the modelling presented below, we did not investigate the dependency of titanite verse rutile stability as a function of XCO_2 at high pressures. However we note that titanite-lawsonite bearing eclogites have been reported previously (e.g. Brovarone, Groppo, Hetényi, Compagnoni, & Malavieille, 2001; Ravna, E. J. K., Torgeir B. Andersen, Laurent Jolivet, and Christian De Capitani, 2010; Brovarone, Groppo & Compagnoni, 2011; Lü, Lifei, Yue & Li, 2019), confirming that titanite rather than rutile can be stable at high pressures. Additionally, the currently available activity–composition model for titanite does not incorporate Fe^{3+} and Al. Consequently, phase equilibria calculations do not appear to correctly predict the stability of titanite in our samples. Therefore, modelling of the eclogite was undertaken in the MnNCKFMASHO system. To maintain consistency, the garnet blueschist was also modelled in the same system.

Modelling in a Ti-free system probably does not significantly affect the modelled phase relations as titanite accounts for <1% of the assemblage for the lawsonite eclogite, and <2% for the retrogressed garnet blueschist. Titanite and rutile were not used in the bulk composition calculations that underpin the modelling. Stilpnomelane is restricted to inclusions in garnet and was not included in the modelling.

Aside from limiting the model system to Ti-free, uncertainties in modelling the *P*–*T* conditions of rocks from bulk rock chemistry are the oxidation state (Fe_2O_3), and water content (H_2O) during the formation of the mineral assemblage. As the eclogite and blueschist are interpreted to be hydrous (as suggested by the presence of abundant phengite, and lawsonite or glaucophane), and probably formed in a water-rich subduction environment (e.g. Martin et al., 2014), they were modelled with water in excess. Oxidation state was constrained from the microprobe chemical analyses used to calculate the metamorphic rock chemistry by assuming mineral stoichiometry in the calculation of cations from raw weight % oxide data (Droop, 1987).

Table 1: Modal proportion estimates for lawsonite eclogite and garnet blueschist, obtained from MLA mapping and then used to calculate bulk rock chemistries for phase equilibria forward models.

		Volume %	Density	Weight %
RB11 Lawsonite eclogite	Garnet	20	4.07	26
	Lawsonite	7	3.08	7
	Omphacite	5	3.38	2
	Glaucophane	10	3.07	9
	Chlorite	10	3.03	9
	Phengite	48	2.93	46
RB12 Garnet blueschist	Garnet	5	4.07	7
	Glaucophane	80	3.07	78
	Phengite	6	2.94	6
	Chlorite	4	2.81	3
	Quartz	3	2.7	2
	Omphacite	1	3.38	1

5. RESULTS

5.1 Electron Probe Micro Analyses

Representative mineral compositions from electron probe analysis are shown in Supplementary Table 1, garnet traverses are in Figure 4. Garnets in both the lawsonite eclogite and retrogressed garnet blueschist have Mn-rich (25-30%) cores and Mn depleted rims, consistent with preservation of prograde zoning (Figure 4). In both samples, X_{Mg} decreases from the core (0.55) to a value of around 0.35. In the lawsonite eclogite grossular increases slightly from core to rim (from 0.23 to 0.3), whereas in the garnet blueschist, grossular decreases slightly from core (0.3) to the rim (0.27). In both samples pyrope contents are low (0-02–0.03) in the garnet core and show a step to 0.05 within 250 µm from the rim in the lawsonite eclogite, and a step to 0.09–0.1 toward the rim of garnet in the blueschist. On average omphacite in the lawsonite eclogite has 39% and 42% jadeite and diopside components respectively, with 11% hedenbergite and 8% aegirine. In the garnet blueschist, omphacite inclusions in garnet contain 36% jadeite, 42% diopside, 3%

hedenbergite and 25% aegerine. Phengite in the lawsonite eclogite shows anti-tschermaks zoning with cores enriched in Al and depleted in Si relative to the rims. Phengite has an average Si content of 3.57 p.f.u. and 3.76 p.f.u. in the lawsonite eclogite and garnet blueschist respectively. There is no major detectable compositional zonation in lawsonite, with Fe and Ti contents less than 1%. In the lawsonite eclogite, retrograde chlorite has an X_{Mg} of 0.62, and retrograde glaucophane has an X_{Mg} of 0.4 and X_{Al}^{iv} of 0.31. In contrast, in the garnet blueschist, glaucophane is consistently zoned with Mg rich-$_{Al}^{vi}$ –rich cores (X_{Mg} = 0.62; X_{Al}^{vi} = 0.35) and comparatively depleted rims (X_{Mg} = 0.57; X_{Al}^{vi} = 0.33). In the garnet blueschist the chlorite X_{Mg} is 0.55.

5.2 LA–ICP–MS mapping

The results of quantitative LA–IC–PMS mapping of lawsonite and garnet are shown in Figure 5. Mapping was done to assist interpretation of Lu–Hf and Sm–Nd geochronology, and the largest grain of lawsonite, or garnet, from each sample was mapped. Inclusions are masked in white, and parts of the grains below the limit of detection (LOD) are shown in black. Garnet has highly Lu enriched cores with respect to rims in both the lawsonite eclogite and the garnet blueschist, consistent with Mn compositional patterns that reflect prograde zoning. In contrast to Lu, Sm concentrations in the lawsonite eclogite do not vary significantly across garnet. In the garnet blueschist there is a suggestion of a slight Sm enrichment in the core. Lu concentrations in lawsonite range between < 0.5–2.5 ppm. In some instances, grains have a distinctly Lu-enriched core, suggesting that Lu may have concentrated into lawsonite prior to the availability of a garnet reservoir. In other grains, the domains of Lu enrichment less obviously coinciding with the cores of the grains.

5.3 Lu–Hf and Sm–Nd geochronology

Lu–Hf and Sm–Nd analyses of garnet, whole rock and lawsonite yield various ages, dependant on the isotopic system used or the mineral separates selected (Figure 6; Supplementary Table 3). The Sm–Nd garnet–whole rock two point isochron from the lawsonite eclogite gives an age of 533.0±9.8 Ma. Three Lu–Hf isochrons can be compared for the lawsonite eclogite: garnet–lawsonite–whole rock, lawsonite–whole rock and garnet–whole rock, yielding ages of 487±11 Ma, 506±15 Ma and 489.7±5.5 Ma respectively. One lawsonite fraction was excluded due to a high $^{176}Lu/^{177}Lu$ ratio (Supplementary Table 3).

The Sm–Nd garnet–whole rock isochron from the garnet blueschist yields an Sm–Nd age of 464.0±3.9 Ma, with the two garnet fractions representing different garnets in the sample. One garnet fraction was excluded from the analyses due to high (7.239 ppm) Nd concentrations resulting in low $^{147}Sm/^{144}Nd$ ratios (Supplementary Table 3), that probably reflects contamination by titanite. The Lu–Hf garnet–whole rock isochron for the garnet blueschist gives an age of 472.4±1.7 Ma. One garnet fraction was excluded due to high Lu and Hf concentrations, which resulted in a low $^{167}Lu/^{177}Hf$ ratio (Supplementary Table 3).

5.4 U–Pb geochronology

In-situ U–Pb dating of zircons was undertaken on the lawsonite eclogite. U–Pb results are in Supplementary Table 4. This rock contains a remarkable number of zircons. They occur as ~1–10 μm inclusions in garnet where they define inclusions trails with titanite (Figure 7a-c). Zircons of 1-10 μm size also occur in the phengite-bearing matrix surrounding the garnet (Figure 7d-e). The zircons are commonly euhedral, showing well developed simple tetragonal forms (Figure 7e). However, despite the large number of zircons in the sample, only a small number were large enough to be analysed. Low U contents and the small size of the zircons made zircon U–Pb dating challenging. Twenty-two analyses of the fifty-five in total were excluded due to high concentrations of ^{204}Pb, that probably reflect incorporation of adjoining minerals and grain boundaries in the analysis, and ten analyses were excluded due to significant discordance. The thirty-three remaining concordant analyses span a range of ages from ca. 560 ± 40 to 440 ± 10 Ma (Figure 8). There is no statistical age difference between zircons that occur as inclusions in garnet and zircons in the matrix, although the comparison is hampered by the generally large individual errors on each analysis. The spread of data points along concordia presents no overt case for Pb loss, as all presented data is concordant. However concordance may be due to large the individual data point errors. Therefore, the spread of ages along concordia could reflect minor Pb-loss.

5.5 Phase equilibria modelling

The lawsonite eclogite RB11 contains the interpreted peak assemblage phengite–garnet– omphacite– lawsonite–quartz (+ titanite). The modelled bulk composition incorporates the entire garnet. Because the garnet is prograde zoned, this bulk composition is useful to estimate garnet nucleation and growth on the prograde path. However, this means it is an approximation for the effective composition at the metamorphic peak and during the formation of the retrograde assemblages. Aside from core enrichment in MnO, the major compositional components in garnet are FeO and CaO. Garnet compositional zoning (Figure 4) shows the outer parts of garnet are comparatively homogeneous in FeO and CaO, and volumetrically this outer domain comprises more than 80% of the garnet volume. Since garnet comprises approximately

15–20% of each sample, the core regions of garnet comprise only a small fraction of the rock volume. Therefore, while modelling the peak assemblage using a composition that includes the garnet cores is obviously an approximation, it is unlikely to negate the general predictions for the peak *P–T* estimation.

The peak assemblage is modelled to occur at ~2.7 GPa and ~590 °C (Figure 9a). The peak field is bound by the conversion of quartz to coesite as well as the conversion of omphacite to jadeite, the lower temperature appearance of talc, and the loss of lawsonite at higher temperature (Figure 9a).

The inferred prograde evolution is marked by the grey dashed arrow. This evolution is based on the inclusions in garnet, which comprise lawsonite, omphacite, glaucophane, epidote, chlorite and quartz. The generalised retrograde evolution is defined by the appearance of glaucophane and chlorite. The retrograde trajectory tracks approximately parallel to lawsonite modal abundance contours, depicted by the grey arrow. This trajectory is based on the appearance of chlorite and glaucophane, while maintaining a lawsonite–garnet–omphacite–quartz assemblage. The *P–T* path passes through talc stability, however the modelled talc modal proportions in this part of *P–T* space are less than 1%, therefore if it formed, it could have easily been removed by continued retrogression and/or be difficult to detect in the presence of the abundant phengite in the sample.

The garnet blueschist RB12 contains the assemblage garnet–glaucophane–phengite–quartz (+rutile) with retrograde chlorite, lawsonite and titanite. The garnets contain abundant omphacite, quartz, glaucophane and phengite inclusions, suggesting omphacite and glaucophane coexisted with garnet during the prograde to peak evolution. There is no omphacite in the glaucophane-rich matrix, suggesting the matrix assemblage may in part be retrograde. The peak mineral assemblage is interpreted as existing in the large garnet–phengite–glaucophane–quartz–jadeite field (Figure 9c). The clinopyroxene inclusions in garnet are omphacitic, however their J value (Na/Na+Ca in the DS5 THERMOCALC model) is 0.61, indicating they are close to the jadeite/omphacite solvus. The modal proportion of garnet and the grossular content of garnet (g(Z)) can also be used as a guide to the potential *P*–*T* conditions. Prior to partial replacement by chlorite, garnet comprised ca. 12% of the sample when converted to one cation normalised proportions to accord with computed modes in DS5, and average grossular (z value in the DS5 THERMOCALC model) content in the outer part of the garnet is 0.24. These plot at approximate *P*–*T* conditions of 2.0 GPa and 550 °C (Figure 9d).

The retrograde evolution is defined by the partial replacement of garnet by chlorite, the loss of omphacite from the matrix, and the appearance of minor lawsonite, with the caveat we have modelled a rock composition that includes the garnet cores. Where retrograde chlorite is in contact with the matrix glaucophane, glaucophane crystals are euhedral, and there is no textural evidence for replacement of the glaucophane, suggesting glaucophane and chlorite were stable on the retrograde path. Therefore, the retrograde evolution probably passed into the garnet–glaucophane–phengite–quartz–chlorite–lawsonite field. This field covers a large range of *P*–*T* conditions, from 1.4–2.8 GPa and 310–510 °C, and it is difficult to pinpoint the exact retrograde P–T trajectory.

6. DISCUSSION

6.1 Timing of high-pressure metamorphism at Port Macquarie

In garnet-bearing low-temperature high-pressure rocks, the Lu–Hf system has proved a reliable geochronomoter, as Lu fractionates into lawsonite and fractionates strongly into garnet, and is less influenced by inclusions than the Sm–Nd system, particularly in mafic rocks which are poor in or devoid of inherited zircons, (Becker, Jochum, & Carlston, 2000; Martin et al., 2009, Mulcahy, Vervoot & Renne, 2014). In the lawsonite eclogite sample RB11, the whole rock and 4 lawsonite fractions give a Lu–Hf age of 506±15 Ma, and the garnet–whole rock gives 489.7±5.5 Ma (Figure 6). Although these are within error of each other, phase equilibria modelling suggests that lawsonite would have nucleated before garnet on the prograde path (Figure 9a), consistent with inclusions of lawsonite in garnet, and the formation of Lu-rich domains within lawsonite. However, the presence of abundant porphyroblasts of both minerals suggest they grew at the same time for a least a part of the metamorphic history. The larger error on the lawsonite-whole rock isochron is due to low $^{176}Lu/^{177}Hf$ ratios of the lawsonite fractions. The garnet–lawsonite–whole rock isochron gives an age of 487±11 Ma (Figure 6c). However, this is controlled by the garnet–whole rock pair, and hence is similar to the garnet–whole rock isochron (489.7±5.5 Ma).

The garnet–whole rock Lu–Hf age is interpreted to record garnet growth, based on the preservation of Lu-rich garnet cores in RB11 (Figure 5a), consistent with prograde growth. The pronounced concentration of Lu in the garnet cores (Figure 5a), indicates that the garnet Lu–Hf age is strongly biased toward the early stage of garnet formation, and therefore better constrains prograde, rather than peak metamorphism. The garnet contains micro-zircon inclusions that span an age range that encompasses the garnet Lu–Hf age. Although the sample preparation method for garnet Lu–Hf analysis involved bench top dissolution rather than high pressure dissolution specifically to minimise inadvertant incorporation of zircon, it is possible that some zircon was incorporated into the TIMS analysis, and could have contributed to the measured Lu–Hf ratios of the garnet. However, quantitative laser ablation maps (Figure 5), show that Lu concentrations in garnet range between 1–11 ppm and Hf concentrations are ca. < 2 ppm across garnet grains. Lu and Hf ppms measured by TIMS are 2.83 and 2.58 respectively (Supplementary Table 3), close to a volumetrically weighted average of Lu–Hf concentrations derived from LA–ICP–MS analysis of garnet grains. Microprobe analyses of zircon from the same sample shows that zircons contain on average 1.08 wt% Hf (Supplementary Table 5). Therefore, while it is possible that some zircon was incoporated into the analysed garnet Lu–Hf aliqouts, it is evident the vast bulk of the analysed Lu and Hf isotopes come from garnet. Similarly, mapped concentrations of Lu in lawsonite show they have on average less than 1.5 ppm Lu, consistent with the TIMS data.

Figure 4 shows the distribution of Lu, Hf, Sm and Nd in examples of garnet and lawsonite from the dated samples. In the lawsonite eclogite, garnets have Lu rich cores whereas Sm is unzoned. However the Sm–Nd age of 533.4±9.8 Ma is significantly older than the ca. 490 Ma Lu–Hf ages (Figure 6). Although great effort was taken to obtain pure mineral seperates, fine-grained inclusions of titanite contain high concentrations of Sm and Nd, and are difficult to remove completely during mineral separation. Furthermore, Sm/Nd ratios in titanite are typically lower than in garnet (Spandler, Hermann, Arculus, & Mavrogenes, 2003), and contamination is therefore likely to lower the ^{147}Sm/^{144}Nd ratio of the analysed garnet aliquot, which may explain the comparatively low ^{147}Sm/^{144}Nd ratio of the analysed garnet compared to typical ratios in garnet (Anczkiewicz, Platt, Thirlwall, & Wakabayashi, 2004; Anczkiewicz et al., 2007). Therefore it is conceivable the Sm–Nd age of 533.4±9.8 Ma reflects to some extent the age of an earlier titanite-bearing mineral assemblage. However, an assumption in isochron geochronology is that analysed materials were initially in isotopic equilibrium at t=0. Therefore, an alternative explanation for the Sm–Nd garnet age that is significantly older than the Lu–Hf age could be that the garnet and whole rock had different $^{143}Nd/^{144}Nd$ ratios at t=0. This could have occurred via the infiltration of isotopically evolved fluids affecting the eclogite matrix after garnet growth, creating isotopic disequilibrium between garnet and matrix minerals (e.g. Blichert-Toft & Frei, 2011). Depending on the repsective $^{143}Nd/^{144}Nd$ ratios, this effect could have resulted in a positive slope on the zero-age garnet-whole rock isochron, producing an invalid age that is older than the Lu–Hf garnet growth age. Therefore, for sample RB11, we conclude that garnet growth occurred at 487±11 Ma.

Garnet in the garnet blueschist gives an Sm–Nd age of 464.0±3.9 Ma and a Lu–Hf age of 472.4±1.7 Ma (Figure 6). The Lu–Hf and Sm–Nd ages are not in error of each other. Lu–Hf closure temperatures are generally considered to be higher than that of the Sm–Nd system (Sm–Nd: ~700°C, Lu–Hf: ~750°C; e.g. Scherer, Cameron, & Blichert-Toft, 2000; Ganguly, Tirone, & Hervig, 1988). However the phase equilibria modelling (Figure 9) suggests peak metamorphic temperatures were lower than closure for both these systems. Hence the difference in ages cannot simply be attributed to differences in closure systematics. The age difference could reflect non-zero t=0 slopes for either isochron. Alternatively, the difference in ages could arise from internal zonation patterns in the garnet (Figure 5). Garnet in RB12 shows enrichment of Lu (14 ppm) in the core, consistent with Rayleigh fractionation during growth (Otamendi, de La Rosa, Douce, & Castro, 2004). However there is no disernable zonation in Sm. The Lu zoning suggests the Lu–Hf age should be biased towards the early stages of garnet growth, whereas the Sm–Nd age is biased toward the outer parts of the garnet simply because of the spherical volumetric relationship (e.g. Lapen et al., 2003; Skora et al., 2006). This notion is consistent with the relative difference between the Lu–Hf and Sm–Nd ages, and if correct, provides some indication of the likely duration over which garnet grew. Therefore, garnet growth in RB12 probably occurred over the period 472.4±1.7 Ma to 464±3.9 Ma.

Although the matrix of the garnet blueschist is interpreted to be largely retrograde in origin due to the presence of omphacite inclusions in garnet and their absence in the matrix, the preservation of prograde zoning in the garnet indicates the Lu–Hf and Sm–Nd ages are not retrograde in origin. Instead, they clearly date prograde metamorphism up to and including the formation of an omphacite-garnet-bearing assemblage.

Comparing the garnet Lu–Hf ages of both samples, it is evident the lawsonite eclogite sample is older than the garnet blueschist. This age difference could reflect that the samples underwent subduction-driven burial at different times, or that the samples shared the same burial history, but that garnet formed at different times due to differences in bulk composition between the samples. Figure 9 shows the garnet-in line (i.e. the first nucleation point of garnet) for the lawsonite eclogite and garnet blueschist. The generalised prograde path for the lawsonite eclogite can be interpereted as having seen garnet nucleation at ca. 0.8–1.4 GPa and ca. 350 °C. The prograde history of the blueschist is unknown, and as such, the *P*–*T* conditions of garnet nucleation cannot be deduced. However, regardless of the prograde path taken by each rock, the garnet in line calculated for the garnet blueschist occurs at similar pressures and temperatures to the lawsonite eclogite (Figure 9c,d). As such, assuming garnet growth was not radically over stepped in the blueschist compared to the lawsonite eclogite, garnet growth should have occurred at approximately the same conditions, and therefore time if both protoliths were subducted together. Therefore we interprete the difference in garnet Lu–Hf ages between the two samples reflects that the protoliths were subducted at different times. A similar scenario has been documented elsewhere, where high-pressure rocks have been dated with Lu–Hf geochronology and span an age range between ca. 105 to 86 Ma, leading to the interpretation they were subducted at different times (Mulcahy, Vervoot & Renne, 2014; Porteau et al., 2018).

The U–Pb data collected from micro-zircons in the lawsonite eclogite spread along concordia (Figure 8), with $^{206}Pb/^{238}U$ ages ranging between ca. 560 ± 40 Ma and 440 ± 10 Ma, suggesting they do not define a single age population. The analysed zircons are euhedral (Figure 7). Texturally the analysed zircons occur in garnet and in the surrounding phengite-rich matrix (Figure 7). Inclusion trails in garnet are defined by zircon and titanite (Figure 7) and form 2D microstructral trends that are discordant to titanite and zircon trails in the surrounding schistose matrix. This implies that zircon formed either in stages or progressively during the metamorphic evolution of the rock. Texturally zircon defining garnet-hosted inclusion trails predates zircon in the matrix. However there is no statistical age difference between the different zircon textural populations. In part this probably reflects the large uncertainties on individual analyses. But it also probably reflects that at least some of the zircons in the matrix formed at the same time as zircons located as inclusions in garnet. The microstructural distrubution is impossible to explain unless the zircon is metamorphic in origin. Therefore it is highly unlikely they were inherited from the eclogite protolith either as igneous or detrital grains. The interpretation that the zircons are metamorphic is consistent with numerous other studies showing zircon can form in eclogite with similar *P*–*T* conditions to those recorded at Port Macquarie (e.g. Tomaschek et al., 2003; Warren, Parrish, Waters & Searle, 2005; Rubatto et al., 2008).

The span in concordant ages from the micro-zircons may reflect low temperature alteration and dissolution-precipitation processes (e.g. Rubatto & Hermann, 2007; Hermann & Rubatto, 2014). Potentially the oldest zircons formed during low-temperature hydrothermal alteration close to the sea floor (Spandler, Hermann & Rubatto, 2004; Pagu, Fanning, Nieto & De Fedrico, 2005; Grimes et al., 2009; Aranovich et al., 2017). The source of zirconium for low-temperature zircon growth can be the breakdown of high-temperature Zr-bearing magmatic minerals such as clinopyroxene (Rubatto, Müntener, Barnhorn & Gregory, 2008), and in this scenario the oldest zircons would pre-date subduction. The zircons close to the age of prograde eclogite metamorphism at ca. 490 Ma could also be attributed to prograde low-temperature dissolution-precipitation during subduction (Tomaschek, Kennedy, Villa, Lagos & Ballhaus, 2003; Tamblyn et al., 2019). Zirconium solubility is increased in silicon rich alkaline fluids, which form with increasing pressure, allowing zirconium to be dissolved and precipitaed from the fluid (Ayers, Zhang, Luo & Peters, 2012; Hermann & Rubatto, 2014). The post ca. 490 Ma zircons may have formed by continued dissolution-precipitation during metamorphic mineral reactions and fluid chemistry changes (e.g. Rubatto, Müntener, Barnhorn & Gregory, 2008), resulting in the continued (re)crystalization of zircon on the retrograde path. Alternatively the post ca. 490 Ma zircons ages may reflect minor Pb-loss.

Nothwithstanding the generalised uncertainties associated with interpretation of the age data discussed above, it is apparent that high-pressure metamorphism is late Cambrian to early Ordovician in age. Therfore the above age data indicate the ca. 251 Ma maximum age for eclogite metamorphism at Port Macquarie suggested by Nutman et al. (2013) is incorrect. Notwithstanding the geological implausibility of this early Triassic age maxima (e.g. Phillips, Offler, Rubatto, & Phillips, 2015), it was argued by Nutman et al. (2013) that the abraded nature of the zircons they analysed from a sample of eclogite indicated a detrital origin, thereby placing an upper age limit on the timing of eclogite metamorphism. However the similarity between the ages obtained by Nutman et al. (2013), and ages of zircons from modern beach sands in the SNEO (Sircombe, 1999), suggests the sample analysed by Nutman et al. (2013) was contaminated with modern beach sand, and therefore does not place an upper age constraint on the timing of high-pressure metamorphism. To test this hypothesis, we analysed zircons separated from the beach sand at the eclogite location and from a beach ~ 1 km to north (Supplementary File 1, Supplementary Table 6). The beach sand zircons are rounded, with abraided morphologies (Supplementary Figure 1) similar to those described by Nutman et al. (2013). Figure 10 shows the distribution of ages obtained from the beach sand at the eclogite location and from a beach 1 km to the north. Also shown is the distribution of beach sand zircons from elsewhere in the SNEO (Sircombe, 1999). For reference, our intepreted age of high-pressure metamorphism is also shown. It is evident the beach sand zircon populations contain significant age groups < 400 Ma, including grains as young as ca. 250 Ma. It is also evident the beach sand zircon age distribution from the eclogite location shares most of the age peaks analysed by Nutman et al. (2013; Figure 10). It could be argued that the beach sand zircons at the eclogite locality could be sourced from the eclogite itself. However the eclogite block is only approximately 8 m^3 in size, and its unlikely it could provide enough zircon to consitute the beach sand zircon population, or provide the beach zircons 1 km and more regionally within the SNEO. Therefore we conclude the maximum age of ca. 250 Ma for high-pressure metamorphism inferred by Nutman et al. (2013) is incorrect, and was based on analysis of a contaminated sample.

Nutman et al. (2013) also obtained a poorly constrained U–Pb age from combined rutile and titanite from an undescribed retrogressed high-pressure rock at Port Macquarie. The upper uncertainty on this age (332±140 Ma) overlaps with the garnet Lu–Hf and Sm–Nd ages (ca. 464–472 Ma) obtained from the garnet blueschist . Therefore this poorly defined age bracket records Ordovician high-pressure metamorphism.

The interpretation that high-pressure metamorphism at Port Macquarie is ca. 500–470 Ma is consistent with the Ordovician (ca. 470 Ma) K–Ar age obtained from phengite in blueschist (Fukui, Watanabe, Itaya, & Leitch, 1995). It is also consistent with the range of ages obtained from high-pressure rocks elsewhere in the SNEO, which are all Cambro-Ordovician in age. U–Pb zircon geochronology from eclogite at Attunga (Figure 1) gives an age of ca. 490 Ma (Figure 11; Phillips, Offler, Rubatto, & Phillips, 2015; Manton, Buckman, Nutman & Bennet, 2017). K–Ar and $^{40}Ar/^{39}Ar$ from blueschist at Pigna Barney and Glenrock (Figure 1) gives ages between ca. 470 and 480 Ma (Figure 11; Fukui, Watanabe, Itaya, & Leitch, 1995; Phillips, Offler, Rubatto, & Phillips, 2015).

6.2 Pressure-temperature conditions during metamorphism

Phase equilibria forward modelling (Figure 9) suggests the peak assemblage in the lawsonite eclogite formed at ca. 2.7 GPa and 590 °C, and in the garnet blueschist at slightly lower *P–T* conditions of ca. 2.0 GPa and 550 °C. The peak eclogite conditions are slightly warmer, however broadly similar, to those suggested by Och et al. (2003), who obtained temperatures of 560±40 °C and pressures between 1.8–2.6 GPa, with subsequent cooling to temperatures between 300–500 °C. Although the use of inclusion assemblages to constrain prograde paths needs to be taken with caution, the garnets in the lawsonite eclogite contain a plethora of inclusions that include lawsonite, glaucophane, clinopyroxene, chlorite, epidote and quartz. These minerals have not all been observed in a single garnet, but nonetheless occur in garnets within a single thin section. Taken in their entirety, this group of inclusions suggests a prograde path that crossed the epidote-lawsonite field, leading initially to loss of epidote from the assemblage, and then at higher *P–T*, the loss of chlorite and followed by glaucophane.

The retrograde evolution of the lawsonite-eclogite is characterised by the formation of glaucophane and chlorite at the expense of garnet and omphacite. There is no textural evidence for the breakdown of lawsonite, suggesting the retrograde evolution approximately followed modal proportion contours of lawsonite. As such, the prograde and retrograde evolution of the lawsonite eclogite tracks along the same *P–T* path. In the garnet blueschist, there is less mineralogical diversity, and the prograde path is poorly constrained. However, inclusions of clinopyroxene and glaucophane and a lack of epidote and paragonite in garnet tentatively point to a prograde path that tracks above 1.4 GPa, although a lack of lawsonite inclusions makes this suggestion speculative. The retrograde evolution involved the stability of glaucophane, lawsonite and chlorite, and loss of omphacite and reduction in garnet abundance. This inferred *P–T* evolution tracks through the same field as the prograde path, remaining above pressures of 1.4 GPa while temperature decreases.

Using a reasoned interpretation of the *P–T* path of the lawsonite eclogite and the garnet blueschist, it appears their prograde evolution tracked through a similar path as their retrograde evolution. These inferred ‘hair-pin’ style *P–T* loops are similar to previously inferred metamorphic evolutions experienced by rocks within subduction channels (Ernst et al., 1988; Porteau et al., 2019). The geothermal gradients recorded by the lawsonite eclogite and garnet blueschist are approximately 245 °C/GPa and 275 °C/GPa and respectively. While the exact retrograde evolutions of the high-pressure rocks are tentative, both must have tracked within the lawsonite stability field in their respective bulk compositions. Preservation of pristine lawsonite-bearing assemblages has been previously interpreted to reflect rapid burial and exhumation (Whitney & Davis, 2006; Tsujimori, Sisson, Liou, Harlow, & Sorensen, 2006; Tsujimori & Ernst, 2014). However, it has also been suggested that slow exhumation along cool geothermal gradients (such as within the subduction channel), also aids in the preservation of lawsonite (Tsujimori, Sisson, Liou, Harlow, & Sorensen, 2006; Tsujimori & Ernst, 2014).

At Port Macquarie, maintenance of cold geothermal conditions during exhumation are supported by the preservation of pristine lawsonite and the formation of stage late aragonite veins that cross-cut the metamorphic mineral assemblages. The timing and depth at which the different-aged lawsonite eclogite and garnet blueschist became juxtaposed is uncertain and there are no direct constraints on the timing of their passage through their inferred retrograde conditions.

6.3 Tectonic framework for high-pressure metamorphism in East Gondwana

There are essentially two models for the development of the Gondwanan orogens in eastern Australia. One model is that formation of the orogens was controlled by a long-lived west-dipping subduction system that progressively migrated oceanward (eastwards) during the Palaeozoic (e.g. Collins, 2002; Phillips & Offler, 2011; Moresi, Betts, Miller, & Cayley, 2014; Phillips, Offler, Rubatto, & Phillips, 2015). This proto-Pacific system created a back-arc regime in which sedimentary sequences accumulated in extensional basins (Collins, 2002; Kemp, Hawkesworth, Collins, Gray, & Blevin, 2009; Moresi, Betts, Miller, & Cayley, 2014). This geodynamically extensional regime was punctuated by transient shortening events that reflected changing dynamics on the subductive margin (e.g. Collins, 2002). Metamorphism accompanying these shortening events was high thermal gradient in character, consistent with thinned back arc lithosphere, and was characterised by voluminous S and I-type magmatism (Collins & Richards, 2008).

The physio-mechanical plausibility of this model has been underpinned by 3D numerical geodynamic experiments. Modelling by Moresi, Betts, Miller, & Cayley (2014) explored the consequence of partial pinning of the East Gondwana margin by the arrival of a small continental collider (Figure 12). Where the margin was not pinned by the collider, slab rollback was associated with arc migration and infilling of an extending back-arc environment. Between ca. 500 Ma and 460 Ma, up to 1500 km of dynamically predicted rollback (Moresi, Betts, Miller, & Cayley, 2014), recreates the complex macroscopic tectonic architecture of Australia’s eastern margin remarkably well, and validates the plausibility of a single long-lived subduction system controlling the geodynamic development of the east Gondwanan margin.

The second model for the development of the east Australian orogens is more complex and involves formation of numerous subduction systems and subduction polarity reversals, coupled with accretion of exotic terrains inferred to comprise parts of the New England Orogen which forms the most outboard of the east Australian orogens (Aitchison & Buckman, 2012; Buckman et al., 2015; Manton, Buckman, Nutman & Bennet, 2017). An element of these tectonic models is that the high-pressure metamorphism at Port Macquarie occurred in the early Triassic (Nutman et al., 2013) in response to terrain accretion. However, the age data presented in this paper shows that high-pressure metamorphism at Port Macquarie is Cambro-Ordovician in age, and not Triassic. Furthermore, recent work (Glen, Saeed, Quinn, & Griffin, 2011; Li, Rosenbaum, Yang, & Hoy, 2015; Hoy & Rosenbaum, 2017), has shown the supposed exotic terrains in this second model are likely to have been derived from cratonic Australia. Given these constraints, the simplest and most geodynamically plausible interpretation is the Australian margin of east Gondwana developed in response to a long-lived west-dipping subduction system that bordered the palaeo-Pacific Ocean and whose locus migrated eastward during the Palaeozoic.

6.4 Accumulation of high-pressure products and spatial translation during slab rollback

The geochronological data from Port Macquarie suggests that high-pressure rocks accumulated in a subduction channel over an interval of at least ca. 20 m.y., as demonstrated by the age difference between garnet in the lawsonite eclogite and the garnet blueschist (Figure 11). Timescales from ca. 515–480 Ma have been suggested for subduction and exhumation of eclogite at Attunga in the SNEO (Phillips, Offler, Rubatto, & Phillips, 2015; Manton, Buckman, Nutman, & Bennet, 2017). K–Ar and $^{40}Ar/^{39}Ar$ geochronology on blueschist facies rocks at Glenrock, Pigna Barney and Port Macquarie (Figure 1) gives ages between 483–470 Ma (Fukui, Watanabe, Itaya, & Leitch, 1995; Phillips, Offler, Rubatto, & Phillips, 2015). These periods between eclogite formation at Attunga and blueschist formation elsewhere in the SNEO have been used to suggest extended durations of subduction metamorphism, albeit the time scale has been derived from across widely separated samples (Figure 11; Phillips, Offler, Rubatto, & Phillips, 2015).

Timeframes of the order determined for the record of high-pressure metamorphism in the Port Macquarie mélange have been suggested for durations of high-pressure metamorphism and accumulation in serpentinite or sediment filled oceanic-hosted subduction systems elsewhere. Examples of long-lived accumulation have been documented in the Carribean (Tsujimori, Sisson, Liou, Harlow, & Sorensen, 2006; Krebs et al., 2008; Krebs, Schertl, Maresch, & Draper, 2011; Schertl et al., 2012). In the Dominican Republic, blocks of eclogite, jadiete blueschist and omphacite blueschist in serpentinite mélange record subduction over ca. 40 m.y., constrained by Lu–Hf, Rb–Sr and $^{40}Ar/^{39}Ar$ age data (Krebs et al., 2008). Within the same system in eastern Cuba, ca. 55 m.y. of subduction and exhumation is recorded from U–Pb zircon and $^{40}Ar/^{39}Ar$ data obtained from six blocks of migmatized amphibolite (Lázaro et al., 2009). White mica and amphibole $^{40}Ar/^{39}Ar$ ages from several high-pressure blocks within the Franciscan Complex suggest that subduction and high-pressure metamorphism spanned at least 80 m.y. (Wakabayashi & Dumitru, 2007). Franciscan eclogites also record ca. 7 m.y. between eclogite and overprinting lawsonite-blueschist metamorphism in the same sample (Anczkiewicz, Platt, Thirlwall, & Wakabayashi, 2004; Mulcahy, King, & Vervoot, 2009). In Zagros, blueschists (some containing lawsonite) record cooling from ca. 90 to 65 Ma from Rb–Sr data (Angiboust, Agard, Glodny, Omrani, & Oncken, 2016), or ca. 105 to 85 Ma from in-situ $^{40}Ar/^{39}Ar$ geochronology (Agard et al., 2006; Monie & Agard, 2009). However in contrast to serpentinite-hosted tectonic blocks, the Zagros high-pressure rocks were exhumed as coherent ‘slices’. In another non-mélange example, lawsonite and non-lawsonite bearing high-pressure rocks in Turkey were dated by Lu–Hf techniques, and show a span of prograde ages between ca. 105 and 86 Ma (Mulcahy, Vervoot & Renne, 2014; Pourteau et al., 2018). This is further supported by $^{40}Ar/^{39}Ar$ data which points to retrograde and prograde high-pressure metamorphism from ca. 100 Ma to ca. 75 Ma (Fornash, Cosca & Whitney, 2016). Finally, in the currently active Mariana subduction system, blueschist from recently erupted serpentinite-mud volcanism on forearc trench slope formed in the Eoecene, pointing to ca. 48 m.y. of residence time in the subduction channel (Tamblyn et al., 2019).

Based on the examples above, and the difference in age and *P–T* conditions recorded by the lawsonite eclogite and garnet blueschist in this study, it seems likely the Port Macquarie mélange records accumulation and mixing of newly subducted material with material that had already been subducted. This accumulation of subduction products is consistent with 2D modelling of serpentinised subduction channels (e.g. Gerya, Stöckhert, & Perchuk, 2002). These models predict mélange can accumulate rocks with different *P–T–t* histories that effectively record different points and times in the evolution of the subduction channel. A further prediction of these models is that widening of the subduction channel and return flow from mantle depths (ca. 80 km) requires timeframes of at least ca. 25 m.y. after the initiation of subduction (Gerya, Stöckhert, & Perchuk, 2002). This may provide some explanation for long timeframes between subduction of material and either its accumulation and/or exhumation.

The ages of the Port Macquarie eclogite and blueschist are similar to the age of serperninite hosted eclogite and blueschist eslewehere in the Southern New England Orogen (SNEO; Fukui, Watanabe, Itaya, & Leitch, 1995; Sano, Offler, Hyodo, & Watanabe, 2004; Och, Leitch, Caprarelli, & Watanabe, 2003; Phillips, 2010; Phillips & Offler, 2011; Phillips, Offler, Rubatto, & Phillips, 2015; Phillips, Offler, Rubatto, & Phillips, 2015; Manton, Buckman, Nutman & Bennet, 2017). These Cambro-Orodvician high-pressure rocks now reside within the forearc system of a Devonian-Carboniferous orogen. Logically, these high-pressure rocks must have been metamorphosed during an older phase of subduction to that which created the younger SNEO. This is aligned with the long-lived west-dipping subduction model for eastern Palaeozoic Australia (e.g. Collins, 2002; Kemp, Hawkesworth, Collins, Gray, & Blevin, 2009; Moresi, Betts, Miller, & Cayley, 2014). Palaeotectonic models sugget late Cambrian-early Ordovician subduction was located much closer to the ancient craton margin (Figure 12). If this is correct, it suggests the high pressure rocks in the SNEO were transported over ca. 1500 km from their initial position of subduction. Moresi, Betts, Miller, & Cayley, (2014) also showed it was thermomechanically feasible for more than 1000 km of eastward trench retreat during the Ordovician and into the early Silurian. Logically this transport occurred during slab roll back while the subduction material was entrained within the subduction channel.

A simplified geodynamic evolution of the Australian margin during the formation and accumulation of the high-pressure rocks in the Port Macquarie mélange is shown in Figure 12. It provides a geodynamic context for the subduction and accumulation of the lawsonite eclogite and garnet blueschist with the tectonic evolution of the upper plate. It also provides a mechanism for translocation of high-pressure rocks now located in the SNEO from their probable formation nearer the margin of cratonic of Australia, to their current position in the forearc system of the youngest and most outboard of the eastern Australian Gondwanan orogens.

The formation of the lawsonite eclogite coincides with the latter stages of the Ross-Delamerian Orogeny (514–490 Ma), which flanks cratonic Australia and forms the oldest and most inboard of the eastern Australian Palaeozoic orogens (Figure 12a; Phillips & Offler, 2011; Phillips, Offler, Rubatto, & Phillips, 2015). Pinning of part of this system by accretion of a continental block led to subsequent eastward slab retreat (Moresi, Betts, Miller, & Cayley, 2014), which allowed opening of a large back arc basin and accumulation of sediments and magmatic rocks on the upper plate (Figure 12b; Glen, Saeed, Quinn, & Griffin, 2011; Phillips, Offler, Rubatto, & Phillips, 2015). On-going subduction is recorded by the garnet blueschist at Port Macquarie (Figure 12b). Unfortunately, subsequent to ca. 470 Ma and prior to final exhumation of the serpentinite mélange in the early Permian (Aitchison et al., 1994), there is no record of the location of the high-pressure material now located at Port Macquarie within the SNEO. However, given the absence of serpentinite detritus in sequences in the SNEO until the Permian (Aitchison et al., 1994), we suggest the high-pressure rocks remained buried in a low temperature environment that allowed the preservation of lawsonite and aragonite-bearing assemblages. The incorporation of the high-pressure rocks into the Devonian–Carboniferous accretionary complex in the SNEO suggests the Cambro–Ordovician subduction products were able to continue their migration outboard until at least the Carboniferous, more than 200 m.y. after they formed (Figure 12d).

7. CONCLUSIONS

Serpentinite mélange at Port Macquarie in the southern New England Fold Belt, eastern Australia, contains blocks of eclogite and blueschist that formed during early Palaeozoic subduction of the Protopacific plate beneath east Gondwana. Lawsonite eclogite formed at around 590 °C and 2.7 GPa, and eclogite now retrogressed to garnet blueschist formed at around 2.0 GPa and 550 °C. Despite their current proximity to each other, garnet Lu–Hf and Sm–Nd dating indicates the high-pressure rocks formed at different times. Lawsonite eclogite formed at ca. 490 Ma, whereas the garnet-omphacite bearing precursor to blueschist formed at ca. 470 Ma. The different ages of eclogite metamorphism indicates progressively created subduction products accumulated within the subduction channel and experienced different *P–T–t* evolutions. This is consistent with numerical modeling that predicts mixing of subduction products within serpentinite-filled subduction channels. The interval over which metamorphism of the high-pressure rocks occurred coincides with subduction rollback on the Australian segment of the east Gondwanan margin. Rollback and migration of the subduction channel appears to have transported the high-pressure rocks more than ca. 1500 km oceanward, where they underwent final exhumation within a younger orogen whose development, while geodynamically associated, was not responsible for the formation of the high-pressure rocks. Thermal durations recorded by oceanic hosted high-pressure low-temperature rocks may encompass tens of millions of years, recording long residence times within subduction channels. Over these timescales, subduction zone migration is likely to occur, potentially transporting subducted rocks large distances prior to their exhumation. The *P–T–t* records of accumulated tectonic blocks in serpentinite mélange provide an avenue to interrogate the thermal histories of palaeosubduction systems as they evolve.

Acknowledgements

We are grateful to Laura Morrissey for assistance with the phase equilibria modelling and to Justin Payne for his assistance with the U–Pb geochronology. Kiara Alessio and Mark

Pearce are thanked for discussions regarding post processing of petrological modelling data. Ben Wade at Adelaide Microscopy is also thanked for his technical assistance with data collection. Diana Zivak is thanked for assisting with acquisition of WDS Zr mapping and BSE imaging of zircon. C. L. Friend and two anonymous reviewers are thanked for their contributions to the manuscript, and Bernardo Cesare is thanked for his editorial handing. This research was in part supported by Australian Research Council grant DP160104637.

References

Agard, P., Yamato, P., Jolivet, L., & Burov, E. (2009). Exhumation of oceanic blueschists and eclogites in subduction zones: timing and mechanisms. *Earth-Science Reviews, 92*(1), 53-79.

Aitchison, J., & Ireland, T. (1995). Age profile of ophiolitic rocks across the Late Palaeozoic New England Orogen, New South Wales: implications for tectonic models. *Australian Journal of Earth Sciences, 42*(1), 11-23.

Anczkiewicz, R., Platt, J. P., Thirlwall, M. F., & Wakabayashi, J. (2004). Franciscan subduction off to a slow start: evidence from high-precision Lu–Hf garnet ages on high grade-blocks. *Earth and Planetary Science Letters, 225*(1), 147-161.

Anczkiewicz, R., Szczepański, J., Mazur, S., Storey, C., Crowley, Q., Villa, I. M., Thirlwall, M. F., & Jeffries, T. E. (2007). Lu–Hf geochronology and trace element distribution in garnet: implications for uplift and exhumation of ultra-high pressure granulites in the Sudetes, SW Poland. *Lithos, 95*(3-4), 363-380.

Anczkiewicz, R., & Thirlwall, M. F. (2003). Improving precision of Sm-Nd garnet dating by H2SO4 leaching: a simple solution to the phosphate inclusion problem. *Geological Society, London, Special Publications, 220*(1), 83-91.

Angiboust, S., Agard, P., Glodny, J., Omrani, J., & Oncken, O. (2016). Zagros blueschists: Episodic underplating and long-lived cooling of a subduction zone. *Earth and Planetary Science Letters, 443*, 48-58.

Aranovich, L. Y., Bortnikov, N., Zinger, T., Borisovskiy, S., Matrenichev, V., Pertsev, A., Sharkov, E., & Skolotnev, S. (2017). Morphology and impurity elements of zircon in the oceanic lithosphere at the Mid-Atlantic ridge axial zone (6°–13° N): Evidence of specifics of magmatic crystallization and postmagmatic transformations. *Petrology, 25*(4), 339-364.

Ayers, J. C., Zhang, L., Luo, Y., & Peters, T. (2012). Zircon solubility in alkaline aqueous fluids at upper crustal conditions. *Geochimica et Cosmochimica Acta, 96*, 18-28.

Baitsch-Ghirardello, B., Gerya, T. V., & Burg, J.-P. (2014). Geodynamic regimes of intra-oceanic subduction: Implications for arc extension vs. shortening processes. *Gondwana Research, 25*(2), 546-560.

Barron, B., Scheibner, E., & Slanskīĭ, E. N. (1976). *A dismembered ophiolite suite at Port Macquarie, New South Wales*: New South Wales Department of Mines.

Bebout, G. E., & Barton, M. D. (2002). Tectonic and metasomatic mixing in a high-T, subduction-zone mélange—insights into the geochemical evolution of the slab–mantle interface. *Chemical Geology, 187*(1-2), 79-106.

Becker, H., Jochum, K. P., & Carlson, R. W. (2000). Trace element fractionation during dehydration of eclogites from high-pressure terranes and the implications for element fluxes in subduction zones. *Chemical Geology, 163*(1), 65-99.

Blichert-Toft, J., & Frei, R. (2001). Complex Sm-Nd and Lu-Hf isotope systematics in metamorphic garnets from the Isua supracrustal belt, West Greenland. *Geochimica et Cosmochimica Acta, 65*(18), 3177-3189.

Brovarone, A. V., Groppo, C., Hetényi, G., Compagnoni, R., & Malavieille, J. (2011). Coexistence of lawsonite-bearing eclogite and blueschist: phase equilibria modelling of Alpine Corsica metabasalts and petrological evolution of subducting slabs. *Journal of Metamorphic Geology, 29*(5), 583-600.

Buckman, S., Nutman, A. P., Aitchison, J. C., Parker, J., Bembrick, S., Line, T., Hidaka, H., & Kamiichi, T. (2015). The Watonga Formation and Tacking Point Gabbro, Port Macquarie, Australia: insights into crustal growth mechanisms on the eastern margin of Gondwana. *Gondwana Research, 28*(1), 133-151.

Carswell, D., Wilson, R., & Zhai, M. (1996). Ultra-high pressure aluminous titanites in carbonate-bearing eclogites at Shuanghe in Dabieshan, central China. *Mineralogical Magazine, 60*(3), 461-471.

Castelli, D., & Rubatto, D. (2002). Stability of Al-and F-rich titanite in metacarbonate: petrologic and isotopic constraints from a polymetamorphic eclogitic marble of the internal Sesia Zone (Western Alps). *Contributions to Mineralogy and Petrology, 142*(6), 627-639.

Collins, W., & Richards, S. (2008). Geodynamic significance of S-type granites in circum-Pacific orogens. *Geology, 36*(7), 559-562.

Collins, W. J. (2002). Nature of extensional accretionary orogens. *Tectonics, 21*(4).

Davis, P. B. (2011). Petrotectonics of lawsonite eclogite exhumation: Insights from the Sivrihisar massif, Turkey. *Tectonics, 30*(1).

Diener, J., & Powell, R. (2012). Revised activity–composition models for clinopyroxene and amphibole. *Journal of Metamorphic Geology, 30*(2), 131-142.

Droop, G. (1987). A general equation for estimating Fe3+ concentrations in ferromagnesian silicates and oxides from microprobe analyses, using stoichiometric criteria. *Mineralogical Magazine, 51*(361), 431-435.

Enami, M., Suzuki, K., Liou, J., & Bird, D. K. (1993). Al-Fe3+ and F-OH substitutions in titanite and constraints on their PT dependence. *European Journal of Mineralogy, 5*(2), 219-231.

Federico, L., Crispini, L., Scambelluri, M., & Capponi, G. (2007). Ophiolite mélange zone records exhumation in a fossil subduction channel. *Geology, 35*(6), 499-502.

Fornash, K. F., Cosca, M. A., & Whitney, D. L. (2016). Tracking the timing of subduction and exhumation using 40 Ar/39 Ar phengite ages in blueschist-and eclogite-facies rocks (Sivrihisar, Turkey). *Contributions to Mineralogy and Petrology, 171*(7), 67.

Fukui, S., Watanabe, T., Itaya, T., & Leitch, E. C. (1995). Middle Ordovician high PT metamorphic rocks in eastern Australia: Evidence from K-Ar ages. *Tectonics, 14*(4), 1014-1020.

Ganguly, J., Tirone, M., & Hervig, R. (1998). Diffusion kinetics of samarium and neodymium in garnet, and a method for determining cooling rates of rocks. *Science, 281*(5378), 805-807.

Gerya, T. (2011). Future directions in subduction modeling. *Journal of Geodynamics, 52*(5), 344-378.

Gerya, T. V., Stöckhert, B., & Perchuk, A. L. (2002). Exhumation of high-pressure metamorphic rocks in a subduction channel: A numerical simulation. *Tectonics, 21*(6).

Glen, R. (2013). Refining accretionary orogen models for the Tasmanides of eastern Australia. *Australian Journal of Earth Sciences*, *60*(3), 315-370.

Glen, R., Saeed, A., Quinn, C., & Griffin, W. (2011). U–Pb and Hf isotope data from zircons in the Macquarie Arc, Lachlan Orogen: Implications for arc evolution and Ordovician palaeogeography along part of the east Gondwana margin. *Gondwana Research, 19*(3), 670-685.

Green, E., Holland, T., & Powell, R. (2007). An order-disorder model for omphacitic pyroxenes in the system jadeite-diopsidehedenbergite-acmite, with applications to eclogitic rocks. *American Mineralogist, 92*(7), 1181-1189.

Green, E., White, R., Diener, J., Powell, R., Holland, T., & Palin, R. (2016). Activity–composition relations for the calculation of partial melting equilibria in metabasic rocks. *Journal of Metamorphic Geology*, *34*(9), 845-869.

Griffin, W., Belousova, E., Shee, S., Pearson, N., & O'reilly, S. (2004). Archean crustal evolution in the northern Yilgarn Craton: U–Pb and Hf-isotope evidence from detrital zircons. *Precambrian Research, 131*(3-4), 231-282.

Grimes, C. B., John, B. E., Cheadle, M. J., Mazdab, F. K., Wooden, J. L., Swapp, S., & Schwartz, J. J. (2009). On the occurrence, trace element geochemistry, and crystallization history of zircon from in situ ocean lithosphere. *Contributions to Mineralogy and Petrology, 158*(6), 757.

Guillot, S., Hattori, K., Agard, P., Schwartz, S., & Vidal, O. (2009). Exhumation processes in oceanic and continental subduction contexts: a review *Subduction zone geodynamics* (pp. 175-205): Springer.

Hermann, J., & Rubatto, D. (2014). Subduction of continental crust to mantle depth: geochemistry of ultrahigh-pressure rocks *Treatise on Geochemistry, 2nd Edition*: Elsevier.

Holland, T., & Powell, R. (1998). An internally consistent thermodynamic data set for phases of petrological interest. *Journal of Metamorphic Geology, 16*(3), 309-343.

Holland, T., & Powell, R. (2011). An improved and extended internally consistent thermodynamic dataset for phases of petrological interest, involving a new equation of state for solids. *Journal of Metamorphic Geology, 29*(3), 333-383.

Hoy, D., & Rosenbaum, G. (2017). Episodic behavior of Gondwanide deformation in eastern Australia: Insights from the Gympie Terrane. *Tectonics*.

Jenkins, R., Landenberger, B., & Collins, W. (2002). Late Palaeozoic retreating and advancing subduction boundary in the New England fold belt, New South Wales. *Australian Journal of Earth Sciences, 49*(3), 467-489.

Kemp, A., Hawkesworth, C., Collins, W., Gray, C., & Blevin, P. (2009). Isotopic evidence for rapid continental growth in an extensional accretionary orogen: The Tasmanides, eastern Australia. *Earth and Planetary Science Letters, 284*(3), 455-466.

Krebs, M., Maresch, W., Schertl, H.-P., Münker, C., Baumann, A., Draper, G., Idleman, B., & Trapp, E. (2008). The dynamics of intra-oceanic subduction zones: a direct comparison between fossil petrological evidence (Rio San Juan Complex, Dominican Republic) and numerical simulation. *Lithos, 103*(1), 106-137.

Krebs, M., Schertl, H.-P., Maresch, W., & Draper, G. (2011). Mass flow in serpentinite-hosted subduction channels: P–T–t path patterns of metamorphic blocks in the Rio San Juan mélange (Dominican Republic). *Journal of Asian Earth Sciences, 42*(4), 569-595.

Lanari, P., Vidal, O., De Andrade, V., Dubacq, B., Lewin, E., Grosch, E. G., & Schwartz, S. (2014). XMapTools: A MATLAB©-based program for electron microprobe X-ray image processing and geothermobarometry. *Computers & Geosciences, 62*, 227-240.

Lapen, T. J., Johnson, C. M., Baumgartner, L. P., Mahlen, N. J., Beard, B. L., & Amato, J. M. (2003). Burial rates during prograde metamorphism of an ultra-high-pressure terrane: an example from Lago di Cignana, western Alps, Italy. *Earth and Planetary Science Letters, 215*(1), 57-72.

Lázaro, C., García-Casco, A., Rojas Agramonte, Y., Kröner, A., Neubauer, F., & Iturralde-Vinent, M. (2009). Fifty-five-million-year history of oceanic subduction and exhumation at the northern edge of the Caribbean plate (Sierra del Convento mélange, Cuba). *Journal of Metamorphic Geology, 27*(1), 19-40.

Li, P., Rosenbaum, G., Yang, J. H., & Hoy, D. (2015). Australian-derived detrital zircons in the Permian-Triassic Gympie terrane (eastern Australia): Evidence for an autochthonous origin. *Tectonics, 34*(5), 858-874.

Lü, Z., Lifei, Z., Yue, J., & Li, X. Ultrahigh-pressure and high-pressure lawsonite eclogites in Muzhaerte, Chinese western Tianshan. *Journal of Metamorphic Geology*.

Ludwig, K. (2003). *User's manual for Isoplot 3.00: a geochronological toolkit for Microsoft Excel*: Kenneth R. Ludwig.

Manton, R. J., Buckman, S., Nutman, A. P., & Bennett, V. C. (2017). Exotic island arc Paleozoic terranes on the eastern margin of Gondwana: Geochemical whole rock and zircon U–Pb–Hf isotope evidence from Barry Station, New South Wales, Australia. *Lithos, 286*, 125-150.

Martin, L., Hermann, J., Gauthiez-Putallaz, L., Whitney, D., Vitale Brovarone, A., Fornash, K., & Evans, N. J. (2014). Lawsonite geochemistry and stability–implication for trace element and water cycles in subduction zones. *Journal of Metamorphic Geology, 32*(5), 455-478.

Moresi, L., Betts, P., Miller, M., & Cayley, R. (2014). Dynamics of continental accretion. *Nature, 508*(7495), 245-248.

Mulcahy, S., Vervoort, J., & Renne, P. (2014). Dating subduction-zone metamorphism with combined garnet and lawsonite Lu–Hf geochronology. *Journal of Metamorphic Geology, 32*(5), 515-533.

Mulcahy, S. R., King, R. L., & Vervoort, J. D. (2009). Lawsonite Lu-Hf geochronology: A new geochronometer for subduction zone processes. *Geology, 37*(11), 987-990.

Nutman, A. P., Buckman, S., Hidaka, H., Kamiichi, T., Belousova, E., & Aitchison, J. (2013). Middle Carboniferous-Early Triassic eclogite–blueschist blocks within a serpentinite mélange at Port Macquarie, eastern Australia: Implications for the evolution of Gondwana's eastern margin. *Gondwana Research, 24*(3-4), 1038-1050.

Och, D., Leitch, E., Caprarelli, G., & Watanabe, T. (2003). Blueschist and eclogite in tectonic melange, port macquarie, new south wales, australia. *Mineralogical Magazine, 67*(4), 609-624.

Och, D. J. (2007). *Eclogite, serpentinite, mélange and mafic intrusive rocks: manifestation of long-lived Palaeozoic convergent margin activity, Port Macquarie, eastern Australia.*

Otamendi, J. E., de La Rosa, J. D., Douce, A. E. P. o., & Castro, A. (2002). Rayleigh fractionation of heavy rare earths and yttrium during metamorphic garnet growth. *Geology, 30*(2), 159-162.

Peacock, S. M. (2003). Thermal structure and metamorphic evolution of subducting slabs. *Geophysical Monograph-American Geophysical Union, 138*, 7-22.

Phillips, G. (2010). Discontinuous or slow exhumation after subduction-evidence from high-pressure rocks in the Peel Manning Fault system. *New England Orogen 2010,* 267.

Phillips, G., & Offler, R. (2011). Contrasting modes of eclogite and blueschist exhumation in a retreating subduction system: The Tasmanides, Australia. *Gondwana Research, 19*(3), 800-811.

Phillips, G., Offler, R., Rubatto, D., & Phillips, D. (2015). High-pressure metamorphism in the southern New England Orogen: Implications for long-lived accretionary orogenesis in eastern Australia. *Tectonics, 34*(9), 1979-2010.

Pourteau, A., Scherer, E. E., Schorn, S., Bast, R., Schmidt, A., & Ebert, L. (2019). Thermal evolution of an ancient subduction interface revealed by Lu–Hf garnet geochronology, Halilbağı Complex (Anatolia). *Geoscience Frontiers, 10*(1), 127-148.

Powell, R., & Holland, T. (1988). An internally consistent dataset with uncertainties and correlations: 3. Applications to geobarometry, worked examples and a computer program. *Journal of Metamorphic Geology*, *6*(2), 173-204.

Puga, E., Fanning, C. M., Nieto, J. M., & De Federico, A. D. (2005). Recrystallization textures in zircon generated by ocean-floor and eclogite-facies metamorphism: a cathodoluminescence and U–Pb SHRIMP study, with constraints from REE elements. *The Canadian Mineralogist, 43*(1), 183-202.

Rawlinson, N., Arroucau, P., Musgrave, R., Cayley, R., Young, M., & Salmon, M. (2014). Complex continental growth along the proto-Pacific margin of East Gondwana. *Geology, 42*(9), 783-786.

Rubatto, D., & Hermann, J. r. (2007). Zircon behaviour in deeply subducted rocks. *Elements, 3*(1), 31-35.

Rubatto, D., Müntener, O., Barnhoorn, A., & Gregory, C. (2008). Dissolution-reprecipitation of zircon at low-temperature, high-pressure conditions (Lanzo Massif, Italy). *American Mineralogist, 93*(10), 1519-1529.

Ruh, J. B., Le Pourhiet, L., Agard, P., Burov, E., & Gerya, T. (2015). Tectonic slicing of subducting oceanic crust along plate interfaces: Numerical modeling. *Geochemistry, Geophysics, Geosystems, 16*(10), 3505-3531.

Sano, S., Offler, R., Hyodo, H., & Watanabe, T. (2004). Geochemistry and chronology of tectonic blocks in serpentinite mélange of the southern New England Fold Belt, NSW, Australia. *Gondwana Research*, *7*(3), 817-831.

Scherer, E. E., Cameron, K. L., & Blichert-Toft, J. (2000). Lu–Hf garnet geochronology: closure temperature relative to the Sm–Nd system and the effects of trace mineral inclusions. *Geochimica et Cosmochimica Acta, 64*(19), 3413-3432.

Sircombe, K. N. (1999). Tracing provenance through the isotope ages of littoral and sedimentary detrital zircon, eastern Australia. *Sedimentary Geology, 124*(1-4), 47-67.

Skora, S., Baumgartner, L. P., Mahlen, N. J., Johnson, C. M., Pilet, S., & Hellebrand, E. (2006). Diffusion-limited REE uptake by eclogite garnets and its consequences for Lu–Hf and Sm–Nd geochronology. *Contributions to Mineralogy and Petrology, 152*(6), 703-720.

Spandler, C., Hermann, J., Arculus, R., & Mavrogenes, J. (2003). Redistribution of trace elements during prograde metamorphism from lawsonite blueschist to eclogite facies; implications for deep subduction-zone processes. *Contributions to Mineralogy and Petrology, 146*(2), 205-222.

Spandler, C., Hermann, J. r., & Rubatto, D. (2004). Exsolution of thortveitite, yttrialite, and xenotime during low-temperature recrystallization of zircon from New Caledonia, and their significance for trace element incorporation in zircon. *American Mineralogist, 89*(11-12), 1795-1806.

Stöckhert, B., & Gerya, T. V. (2005). Pre-collisional high pressure metamorphism and nappe tectonics at active continental margins: A numerical simulation. *Terra Nova, 17*(2), 102-110.

Tamblyn, R., Zack, T., Schmitt, A., Hand, M., Kelsey, D., Morrissey, L., Pabst, S., & Savov, I. (2019). Blueschist from the Mariana forearc records long-lived residence of material in the subduction channel. *Earth and Planetary Science Letters, 519*, 171-181.

Tomaschek, F., Kennedy, A. K., Villa, I. M., Lagos, M., & Ballhaus, C. (2003). Zircons from Syros, Cyclades, Greece—recrystallization and mobilization of zircon during high-pressure metamorphism. *Journal of Petrology, 44*(11), 1977-2002.

Tsujimori, T., & Ernst, W. (2014). Lawsonite blueschists and lawsonite eclogites as proxies for palaeo-subduction zone processes: a review. *Journal of Metamorphic Geology, 32*(5), 437-454.

Tsujimori, T., Sisson, V. B., Liou, J. G., Harlow, G. E., & Sorensen, S. S. (2006). Very-low-temperature record of the subduction process: A review of worldwide lawsonite eclogites. *Lithos, 92*(3), 609-624.

Vitale Brovarone, A., Groppo, C. T., Hetényi, G., Compagnoni, R., & Malavieille, J. (2011). Coexistence of lawsonite-bearing eclogite and blueschist: phase equilibria modelling of Alpine Corsica metabasalts and petrological evolution of subducting slabs.

Warren, C. J., Parrish, R. R., Waters, D. J., & Searle, M. P. (2005). Dating the geologic history of Oman's Semail ophiolite: Insights from U-Pb geochronology. *Contributions to Mineralogy and Petrology, 150*(4), 403-422.

Wei, C., & Clarke, G. (2011). Calculated phase equilibria for MORB compositions: a reappraisal of the metamorphic evolution of lawsonite eclogite. *Journal of Metamorphic Geology, 29*(9), 939-952.

White, R., Powell, R., & Holland, T. (2007). Progress relating to calculation of partial melting equilibria for metapelites. *Journal of Metamorphic Geology, 25*(5), 511-527.

Whitney, D. L., & Davis, P. B. (2006). Why is lawsonite eclogite so rare? Metamorphism and preservation of lawsonite eclogite, Sivrihisar, Turkey. *Geology, 34*(6), 473-476.

Figure captions

Figure 1: a) Simplified tectonic map of Eastern Australia showing the main eastwards-younging orogens and high-pressure localities. Study area is indicated in black box. b) Geological map of the Southern New England Fold Belt, indicating the Port Macquarie locality in black box. Yellow stars indicate other high-pressure rock localities (e.g. Phillips, Offler, Rubatto & Phillips, 2015). PMFS: Peel Manning Fault System. c) The Port Macquarie mélange showing the high-pressure metamorphic blocks encased in serpentinite, modified from Och, Leitch, Caprarelli, & Watanabe (2003).

Figure 2: Field photographs of high-pressure rocks from Port Macquarie. a) High-pressure rocks eroded from mélange, showing locations of lawsonite eclogite and garnet blueschist. b) Lawsonite-garnet bearing eclogite with matrix phengite and coarse grained omphacite. c) Garnet blueschist derived from eclogite. The garnet porphyroblasts are partially replaced by chlorite.

Figure 3: Photomicrographs of the samples taken in plane polarised light. a) Lawsonite eclogite showing porphyroblastic lawsonite, omphacite and garnet, with fine grained titanite in phengite-rich matrix. b) Retrograde chlorite and glaucophane in lawsonite eclogite. c) Omphacite, epidote and stilpnomelane inclusions in garnet in the lawsonite eclogite. d) Inclusions of glaucophane and epidote in porphyroblastic lawsonite in the lawsonite eclogite. e) Porphyroblastic garnet in glaucophane-phengite matrix in garnet blueschist. f) Omphacite and glaucophane inclusions within a garnet rim from garnet blueschist.
Abbreviations: Chl: Chlorite, Ep: Epidote, G: Garnet, Gl: Glaucophane, Law: Lawsonite, O: Omphacite, Phe: Phengite, Ru: Rutile, Ttn: Titanite.

Figure 4: EPMA profiles across garnet. a) Zoning profile across garnet from lawsonite eclogite RB11, showing prograde zoning in spessartine and almandine. b) Zoning profile across garnet from garnet blueschist RB12, demonstrating less obvious prograde zoning. Garnets are more fractured in this sample hence the sparsity of data.

Figure 5: LA-ICP-MS element maps of metamorphic minerals targeted for geochronology. Inclusions are masked in white, parts of the grain below LOD are black. a) Lu map of a garnet from lawsonite eclogite showing a pronounced enrichment of Lu in the core. b) Sm map of the same garnet from the lawsonite eclogite, showing no discernible zoning. c) Lu map of a garnet from garnet blueschist, showing enrichment in the core. d) Sm map of the same garnet from the garnet blueschist, showing no discernible zoning. e) Lu map of several lawsonite crystals in lawsonite eclogite sample.

Figure 6: Lu-Hf and Sm-Nd isochrons for lawsonite eclogite and garnet blueschist. a) Sm–Nd isochron for lawsonite eclogite. b) Lu–Hf isochron for lawsonite and whole rock points from lawsonite eclogite. c) Lu–Hf isochron for the garnet and whole rock points for lawsonite eclogite. d) Lu–Hf isochron for all lawsonite, garnet and whole rock points for lawsonite eclogite. e) Lu–Hf isochron for garnet blueschist. f) Sm–Nd isochron for garnet blueschist.

Figure 7: BSE images and Zr map of metamorphic micro-zircons target for U–Pb geochronology. a) WDS electron microprobe Zr map of a garnet and surrounding matrix with Zr hotspots shown in white, white line indicates the outline of the garnet crystal. The identity of the Zr hotspots as zircon has been confirmed with EDS. Inclusion trails of zircon within garnet and within the external foliation wrapping garnet can be seen. The X-

ray map may somewhat over emphasize the size of the zircons, as zircon is vastly richer in Zr compared to host garnet. Nonetheless the image depicts the foliated distribution of the zircon grains. (b) Zircon in garnet rim and surround phengite rich matrix. (c) Zircon inclusion in garnet. (d) Trail of zircon forming in phengite and with titanite. (e) Euhedral zircons forming in a phengite cleavage plane. Abbreviations: G: Garnet, O: Omphacite, Phe: Phengite, Ttn: Titanite, Zrc: Zircon.

Figure 8: a) Terra-Wasserburg plot of U–Pb data from microzircons in lawsonite eclogite. b) Range of zircon U–Pb ages. The horizontal shaded rectangle is the age of peak high-pressure metamorphism of the lawsonite eclogite, inferred in the study from garnet and lawsonite Lu–Hf geochronology.

Figure 9: Phase equilibria forward models calculated with THERMOCALC DS5. Important mineral stabilities are indicated in thicker black lines (garnet-in and lawsonite-in). Grey dashed line indicated the location of a solvus. Yellow star marks the interpreted peak *P–T* conditions reached by each sample, while grey dashed arrows indicate a tentative prograde *P–T* evolution. a) Model for lawsonite eclogite. b) Simplified version of the lawsonite eclogite model, showing interpreted prograde, and peak fields. c) Model for garnet blueschist. d) Simplified version of the garnet blueschist model, showing *P–T* location of interpreted peak and assemblage. Transparent purple fields indicate estimated peak garnet modal proportion and range of measured grossular contents of garnet rims (G(Z)), used to constrain the peak *P–T* conditions. Act: Actinolite, Bi: Biotite, Chl: Chlorite, Coe: Coesite, Cu: Cummingtonite, Ep: Epidote, G: Garnet, Gl: Glaucophane, Hb: Hornblende, Jd: Jadeite,

Law: Lawsonite, O: Omphacite, Pa: Paragonite, Phe: Phengite, Pl: Plagioclase, Q: Quartz, Ta: Talc.

Figure 10: Comparisons between modern beach sand zircon ages at Port Macquarie and the zircon ages interpreted by Nutman et al. (2013) to be detrital in origin, derived from the eclogite at Port Macquarie. Also shown for reference (in dark green) are modern beach sand zircon ages at Coffs Harbour within the SNEO, 150 km north of Port Macquarie (Sircombe, 1999). a) Modern beach sand zircons from Town Beach ca. 1 km north of the eclogite location. b) Modern beach sand zircons from the eclogite locality. c) The zircon age distribution reported by Nutman et al. (2013). Shown in pale green are common zircon age peaks between modern beach sand zircons and the zircon ages reported by Nutman et al. (2013). Shown in grey is the age of eclogite metamorphism determined from this study.

Figure 11: Summary of geochronology on high-pressure rocks exhumed via the Peel Manning Fault System in the SNEO.

Figure 12: Simplified geodynamic model for the evolution of the east Gondwanan margin throughout the Palaeozoic. Left hand panels show the location and style of crust-building, with the collision of a continental block after Moresi, Betts, Miller, & Cayley (2014). Right hand panels show a cross-section through a model subduction zone with the location of the lawsonite eclogite and garnet blueschist adapted from numerical models by Gerya, Stöckhert, & Perchuk (2002). a) During the Ross/Delamerian Orogen, the lawsonite eclogite is formed. b) Slab rollback followed the termination of the Ross/Delamerian Orogen. The garnet blueschist is subducted, and the collision of a continental block affects the southern margin. c) Rollback continues, the eclogites are trapped within the subduction channel

however their depth is unknown. d) The New England Orogen initiates ca. 160 Ma later, the high-pressure rocks are exhumed within their hosting serpentinite, at least ca. 1500 km from the location of their initial subduction.

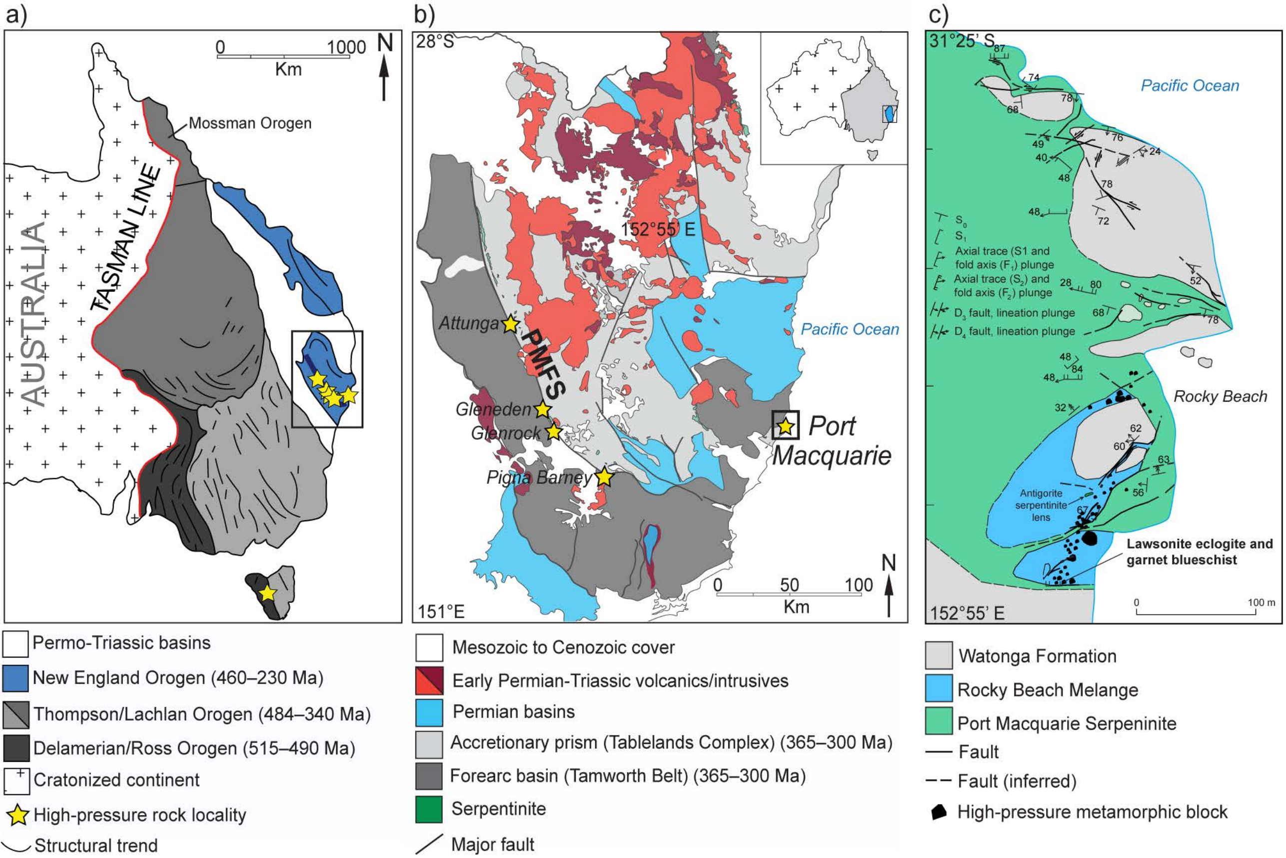
a)
0 1000
Km
N
Mossman Orogen
TASMAN LINE
AUSTRALIA
Permo-Triassic basins
New England Orogen (460–230 Ma)
Thompson/Lachlan Orogen (484–340 Ma)
Delamerian/Ross Orogen (515–490 Ma)
Cratonized continent
High-pressure rock locality
Structural trend
b)
28°S
152°55' E
Attunga
PMFS
Gleneden
Glenrock
Pigna Barney
Port Macquarie
Pacific Ocean
0 50 100
Km
N
151°E
Mesozoic to Cenozoic cover
Early Permian-Triassic volcanics/intrusives
Permian basins
Accretionary prism (Tablelands Complex) (365–300 Ma)
Forearc basin (Tamworth Belt) (365–300 Ma)
Serpentinite
Major fault
c)
31°25' S
Pacific Ocean
S_0
S_1
Axial trace (S1 and fold axis (F_1) plunge
Axial trace (S_2) and fold axis (F_2) plunge
D_3 fault, lineation plunge
D_4 fault, lineation plunge
Rocky Beach
Antigorite serpentinite lens
Lawsonite eclogite and garnet blueschist
0 100 m
152°55' E
Watonga Formation
Rocky Beach Melange
Port Macquarie Serpeninite
Fault
Fault (inferred)
High-pressure metamorphic block

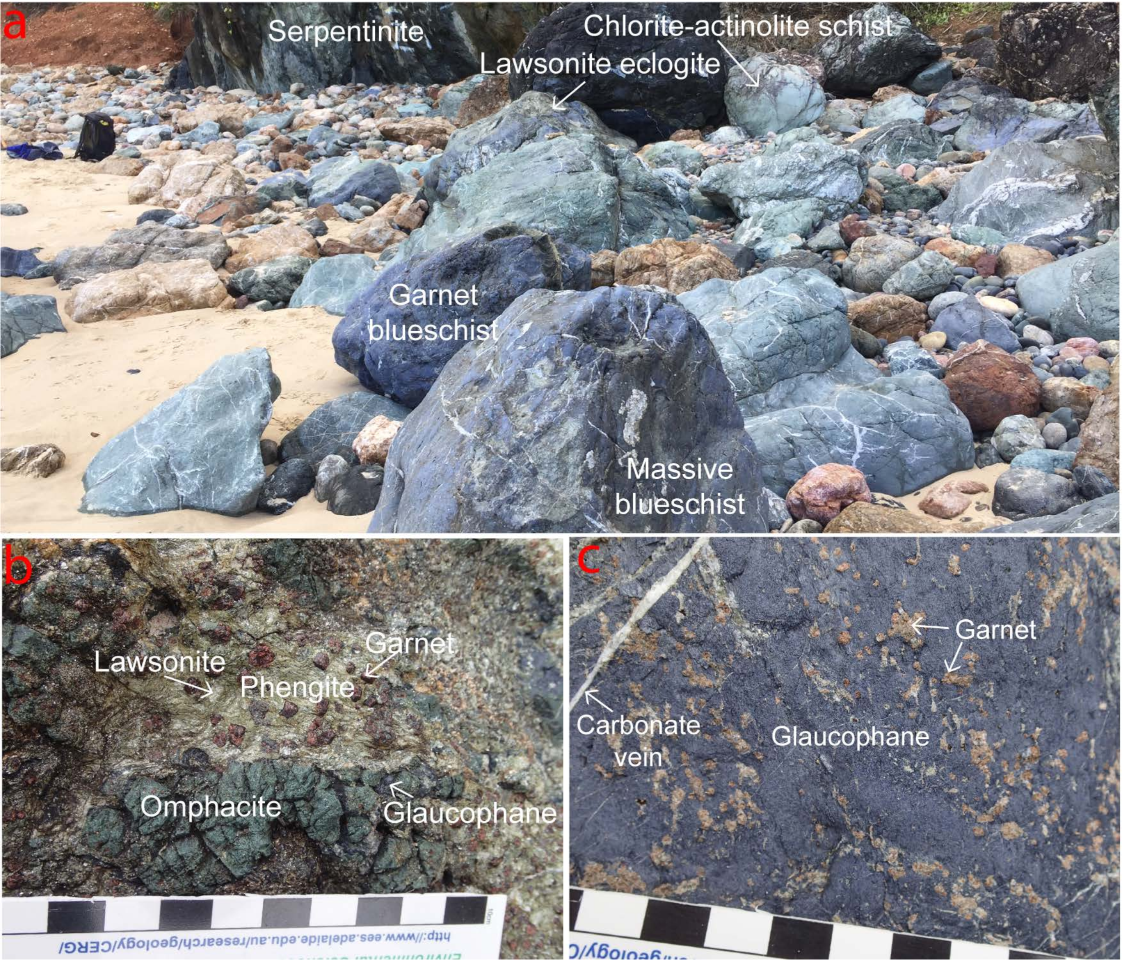
a
Serpentinite
Chlorite-actinolite schist
Lawsonite eclogite
Garnet blueschist
Massive blueschist
b
Lawsonite
Phengite
Garnet
Omphacite
Glaucophane
http://www.ees.adelaide.edu.au/research/geology/CERG/
c
Garnet
Carbonate vein
Glaucophane

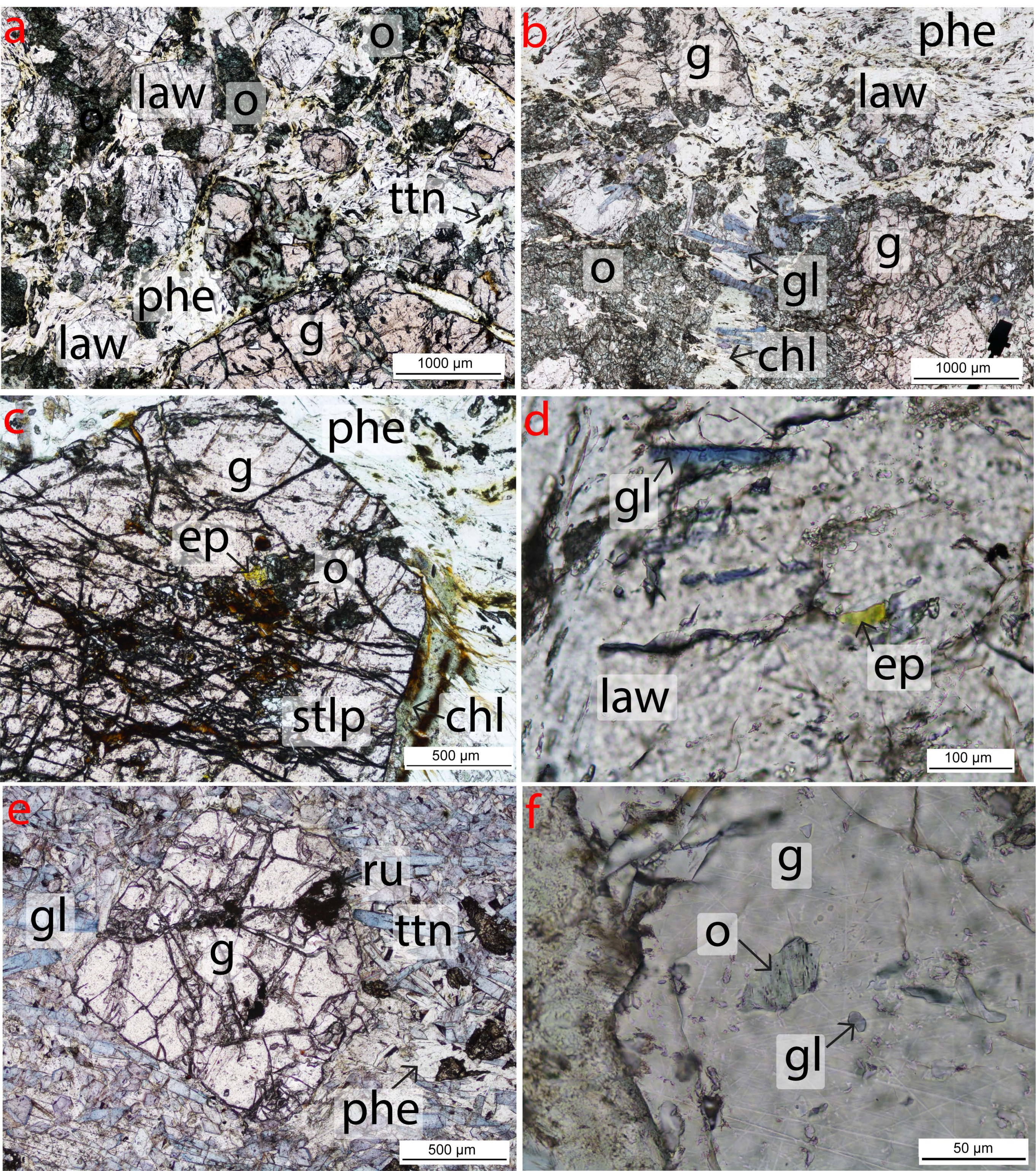
a
law
o
o
o
ttn
phe
law
g
1000 µm
b
phe
g
law
g
o
gl
chl
1000 µm
c
phe
g
ep
o
stlp
chl
500 µm
d
gl
ep
law
100 µm
e
ru
gl
ttn
g
phe
500 µm
f
g
o
gl
50 µm

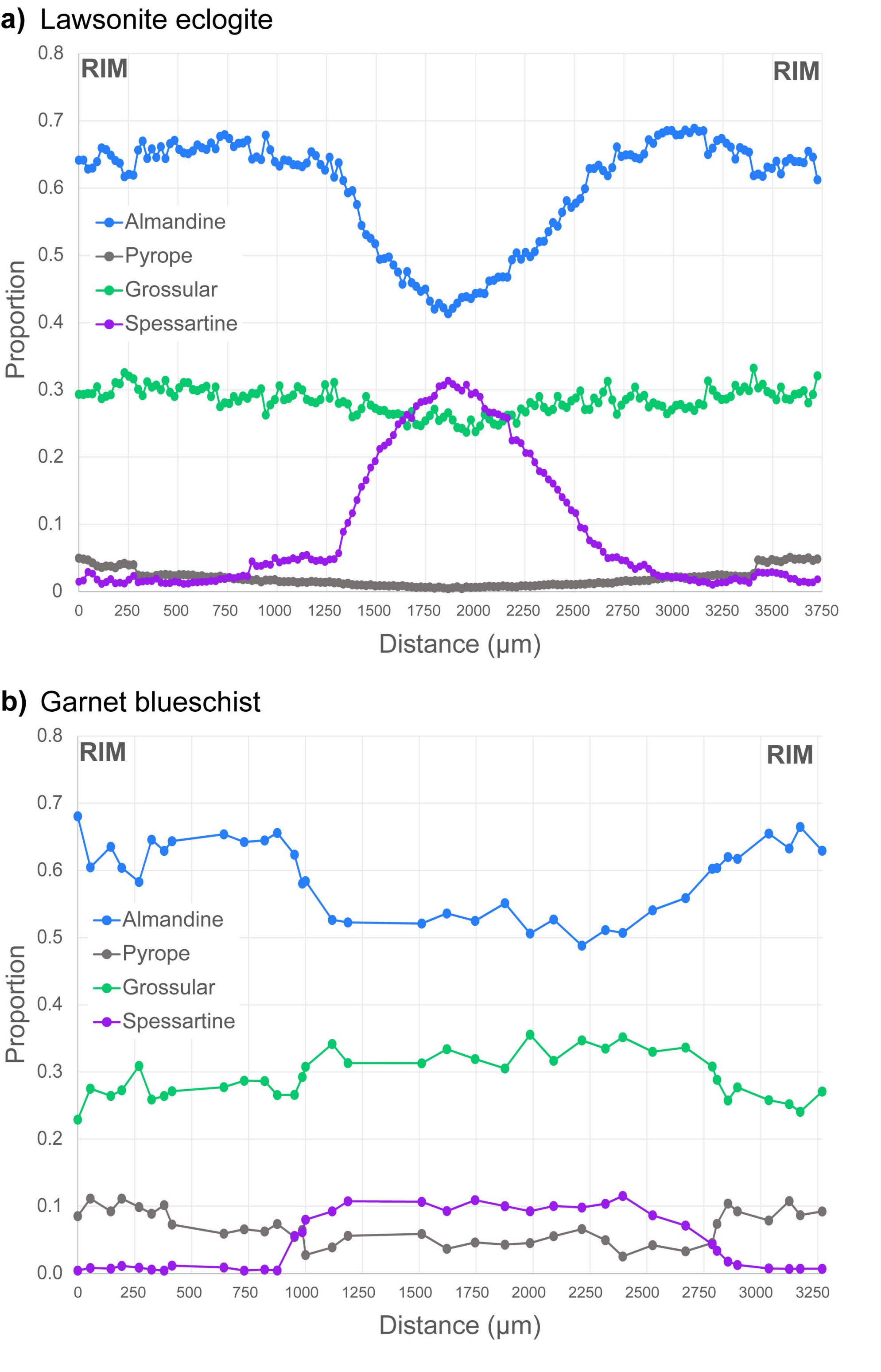

a) Lawsonite eclogite
RIM
RIM
Almandine
Pyrope
Grossular
Spessartine
Proportion
Distance (µm)
0
0.1
0.2
0.3
0.4
0.5
0.6
0.7
0.8
0
250
500
750
1000
1250
1500
1750
2000
2250
2500
2750
3000
3250
3500
3750
b) Garnet blueschist
RIM
RIM
Almandine
Pyrope
Grossular
Spessartine
Proportion
Distance (µm)
0.0
0.1
0.2
0.3
0.4
0.5
0.6
0.7
0.8
0
250
500
750
1000
1250
1500
1750
2000
2250
2500
2750
3000
3250

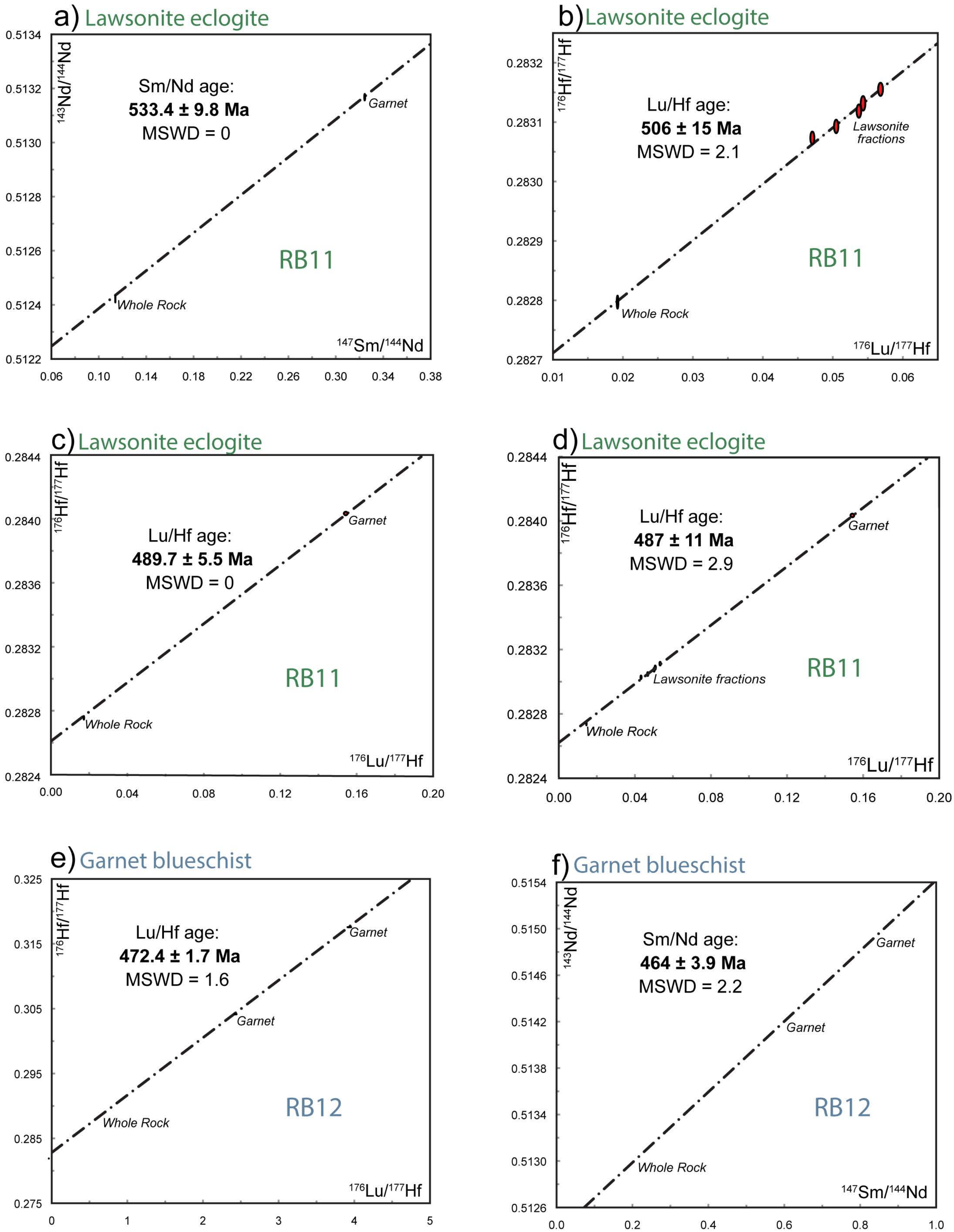

a) Lawsonite eclogite
Sm/Nd age:
533.4 ± 9.8 Ma
MSWD = 0
Garnet
Whole Rock
RB11
$^{143}Nd/^{144}Nd$
$^{147}Sm/^{144}Nd$
b) Lawsonite eclogite
Lu/Hf age:
506 ± 15 Ma
MSWD = 2.1
Lawsonite fractions
Whole Rock
RB11
$^{176}Hf/^{177}Hf$
$^{176}Lu/^{177}Hf$
c) Lawsonite eclogite
Lu/Hf age:
489.7 ± 5.5 Ma
MSWD = 0
Garnet
Whole Rock
RB11
$^{176}Hf/^{177}Hf$
$^{176}Lu/^{177}Hf$
d) Lawsonite eclogite
Lu/Hf age:
487 ± 11 Ma
MSWD = 2.9
Garnet
Lawsonite fractions
Whole Rock
RB11
$^{176}Hf/^{177}Hf$
$^{176}Lu/^{177}Hf$
e) Garnet blueschist
Lu/Hf age:
472.4 ± 1.7 Ma
MSWD = 1.6
Garnet
Garnet
Whole Rock
RB12
$^{176}Hf/^{177}Hf$
$^{176}Lu/^{177}Hf$
f) Garnet blueschist
Sm/Nd age:
464 ± 3.9 Ma
MSWD = 2.2
Garnet
Garnet
Whole Rock
RB12
$^{143}Nd/^{144}Nd$
$^{147}Sm/^{144}Nd$

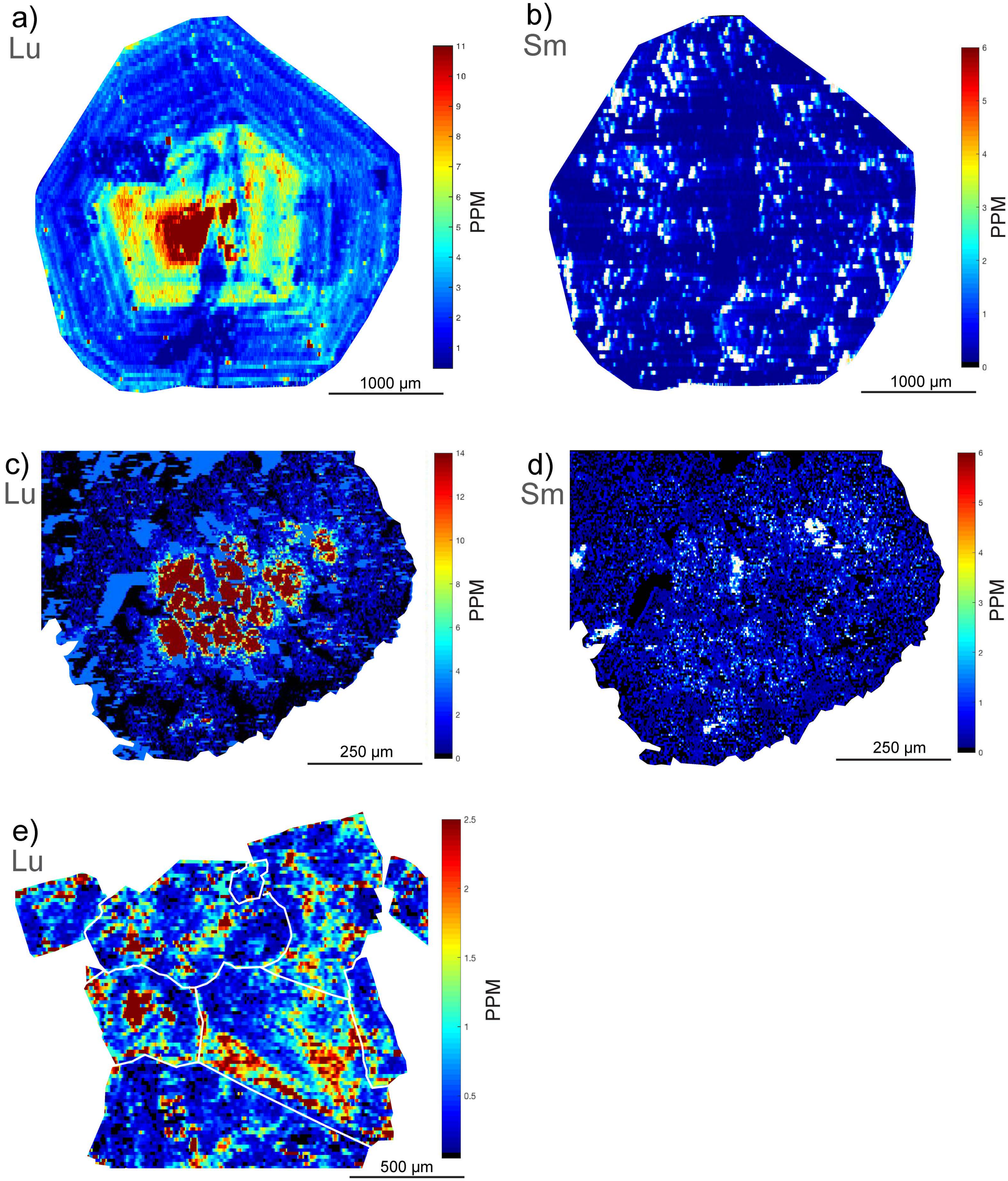

a)
Lu
PPM
1000 µm
b)
Sm
PPM
1000 µm
c)
Lu
PPM
250 µm
d)
Sm
PPM
250 µm
e)
Lu
PPM
500 µm

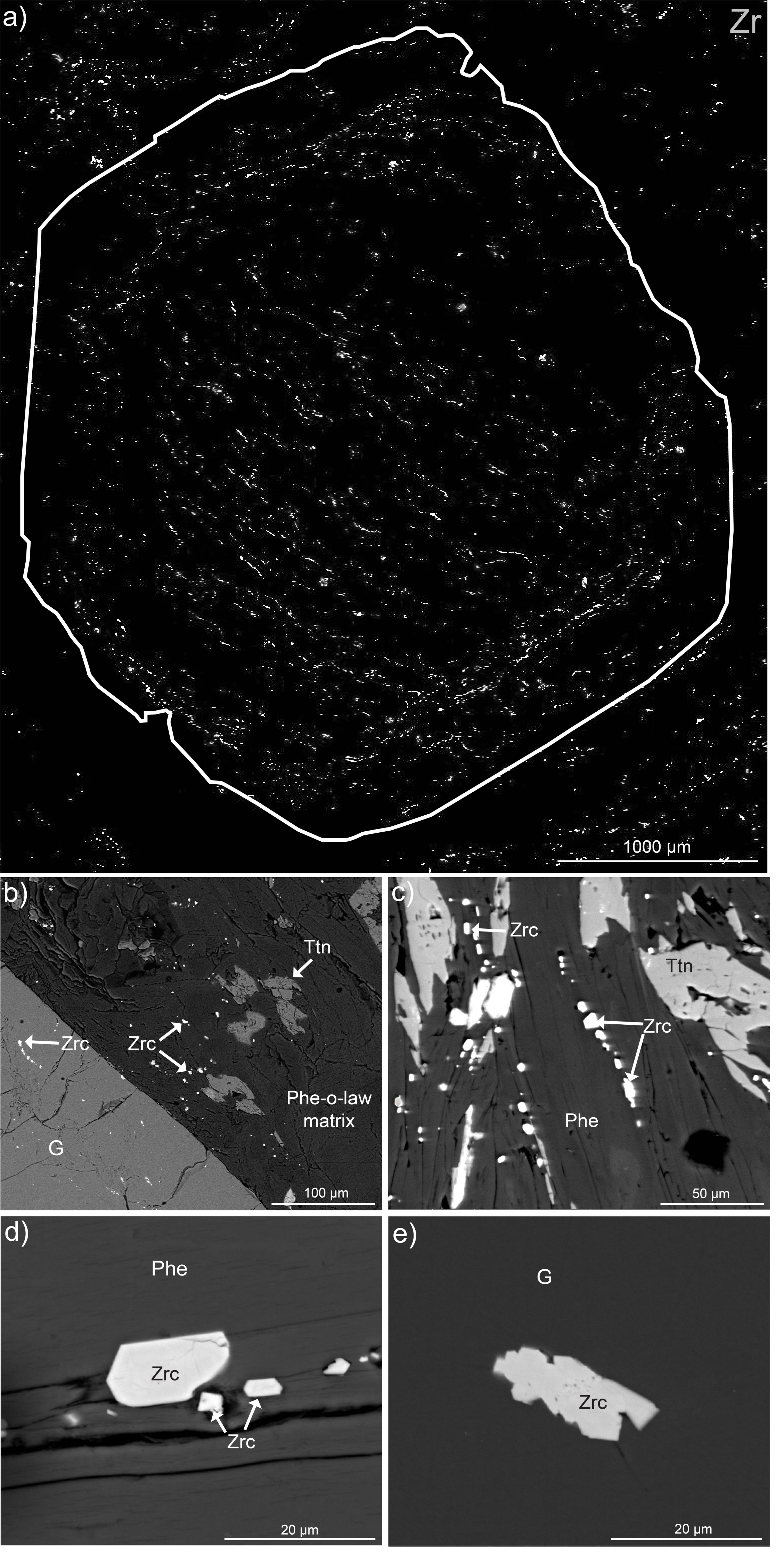

a)
Zr
1000 µm
b)
Ttn
Zrc
Zrc
Phe-o-law
matrix
G
100 µm
c)
Zrc
Ttn
Zrc
Phe
50 µm
d)
Phe
Zrc
Zrc
20 µm
e)
G
Zrc
20 µm

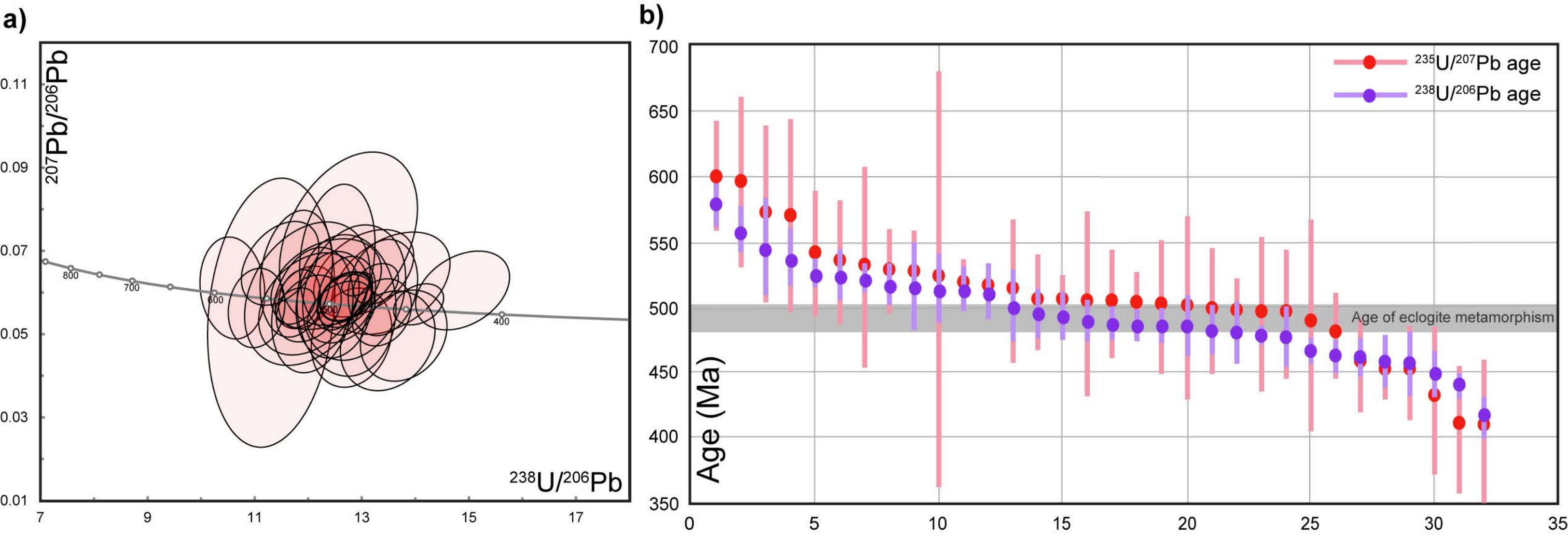
a)
^{207}Pb/^{206}Pb
^{238}U/^{206}Pb
0.11
0.09
0.07
0.05
0.03
0.01
7
9
11
13
15
17
800
700
600
500
400
b)
^{235}U/^{207}Pb age
^{238}U/^{206}Pb age
Age of eclogite metamorphism
Age (Ma)
700
650
600
550
500
450
400
350
0
5
10
15
20
25
30
35

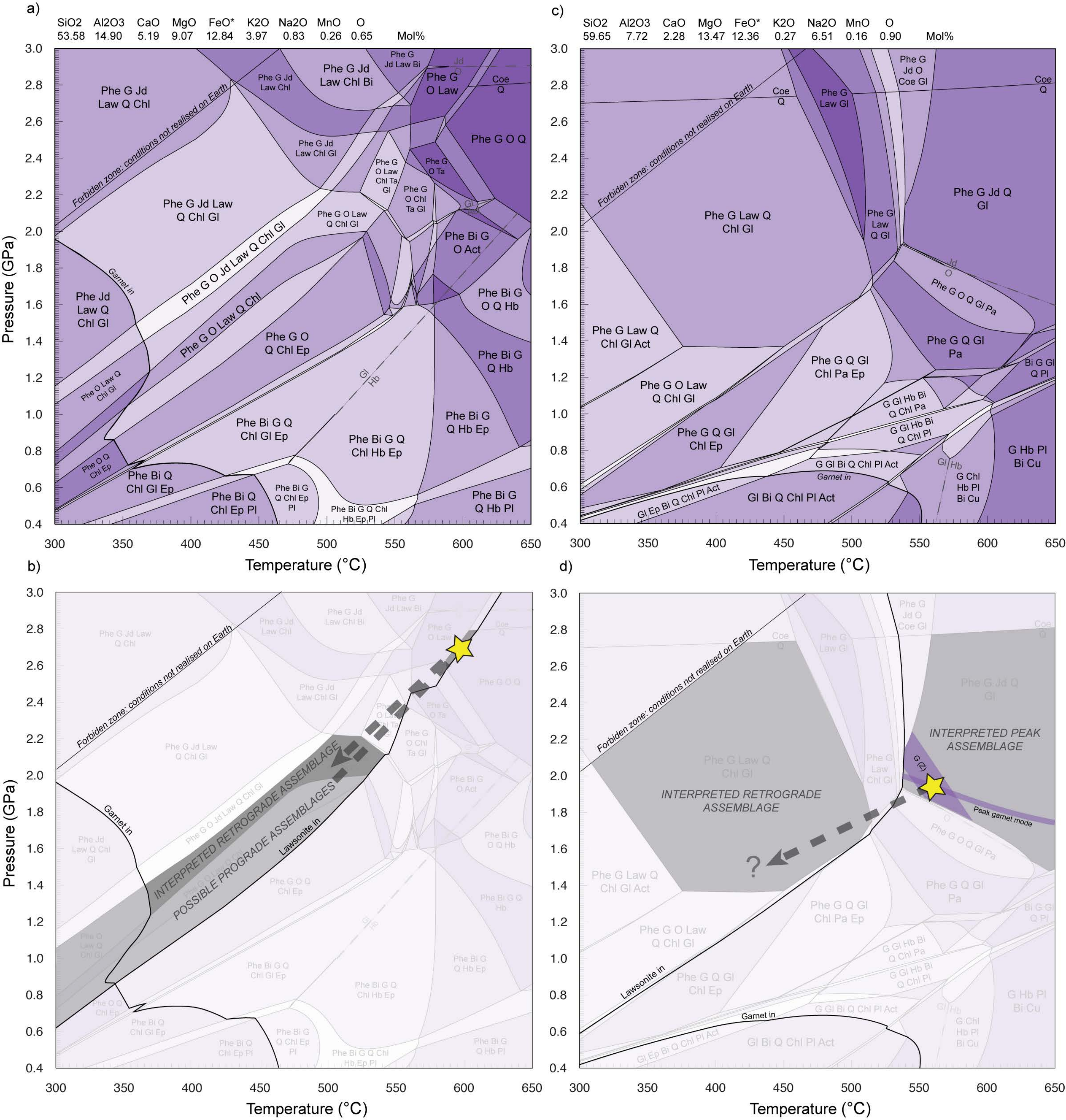

Interpreted peak assemblage: Phe G O Q Law

Possible prograde assemblages: Phe O Law Q ± G Chl Gl Ep

Interpreted retrograde assemblage: Phe G O Law Q Chl Gl

Interpreted peak assemblage: Phe G Jd Gl Q

Interpreted retrograde assemblage: Phe G Gl Q Chl Law

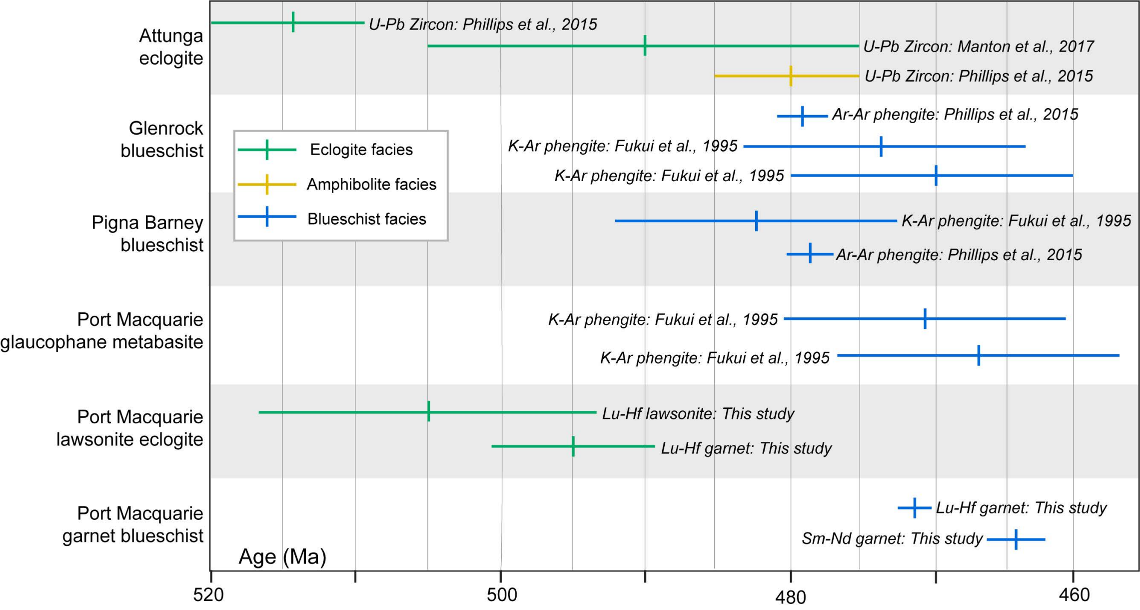

Attunga eclogite
U-Pb Zircon: Phillips et al., 2015
U-Pb Zircon: Manton et al., 2017
U-Pb Zircon: Phillips et al., 2015
Glenrock blueschist
Ar-Ar phengite: Phillips et al., 2015
K-Ar phengite: Fukui et al., 1995
K-Ar phengite: Fukui et al., 1995
Eclogite facies
Amphibolite facies
Blueschist facies
Pigna Barney blueschist
K-Ar phengite: Fukui et al., 1995
Ar-Ar phengite: Phillips et al., 2015
Port Macquarie glaucophane metabasite
K-Ar phengite: Fukui et al., 1995
K-Ar phengite: Fukui et al., 1995
Port Macquarie lawsonite eclogite
Lu-Hf lawsonite: This study
Lu-Hf garnet: This study
Port Macquarie garnet blueschist
Lu-Hf garnet: This study
Sm-Nd garnet: This study
Age (Ma)
520
500
480
460

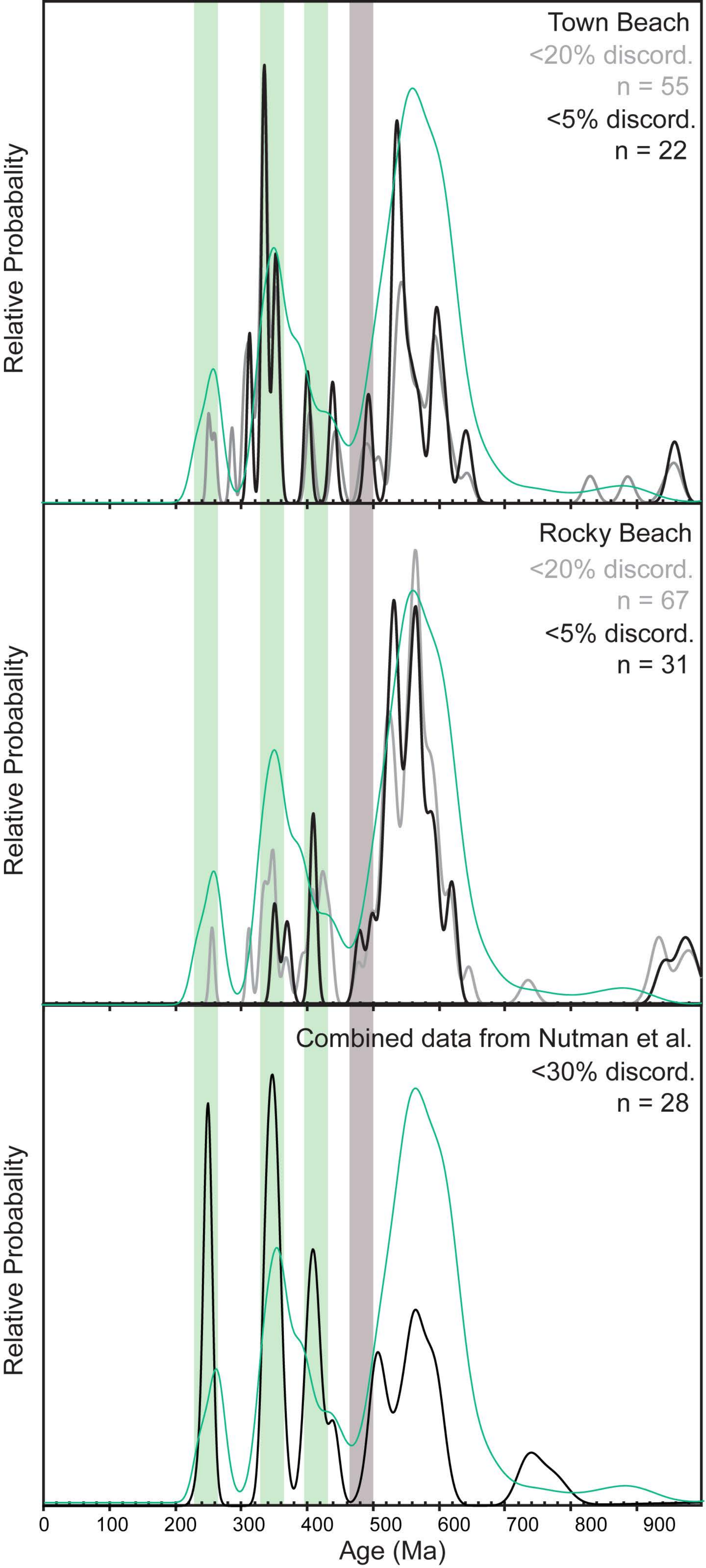

Town Beach
<20% discord.
n = 55
<5% discord.
n = 22
Rocky Beach
<20% discord.
n = 67
<5% discord.
n = 31
Combined data from Nutman et al.
<30% discord.
n = 28
Relative Probabality
Relative Probabality
Relative Probabality
0
100
200
300
400
500
600
700
800
900
Age (Ma)

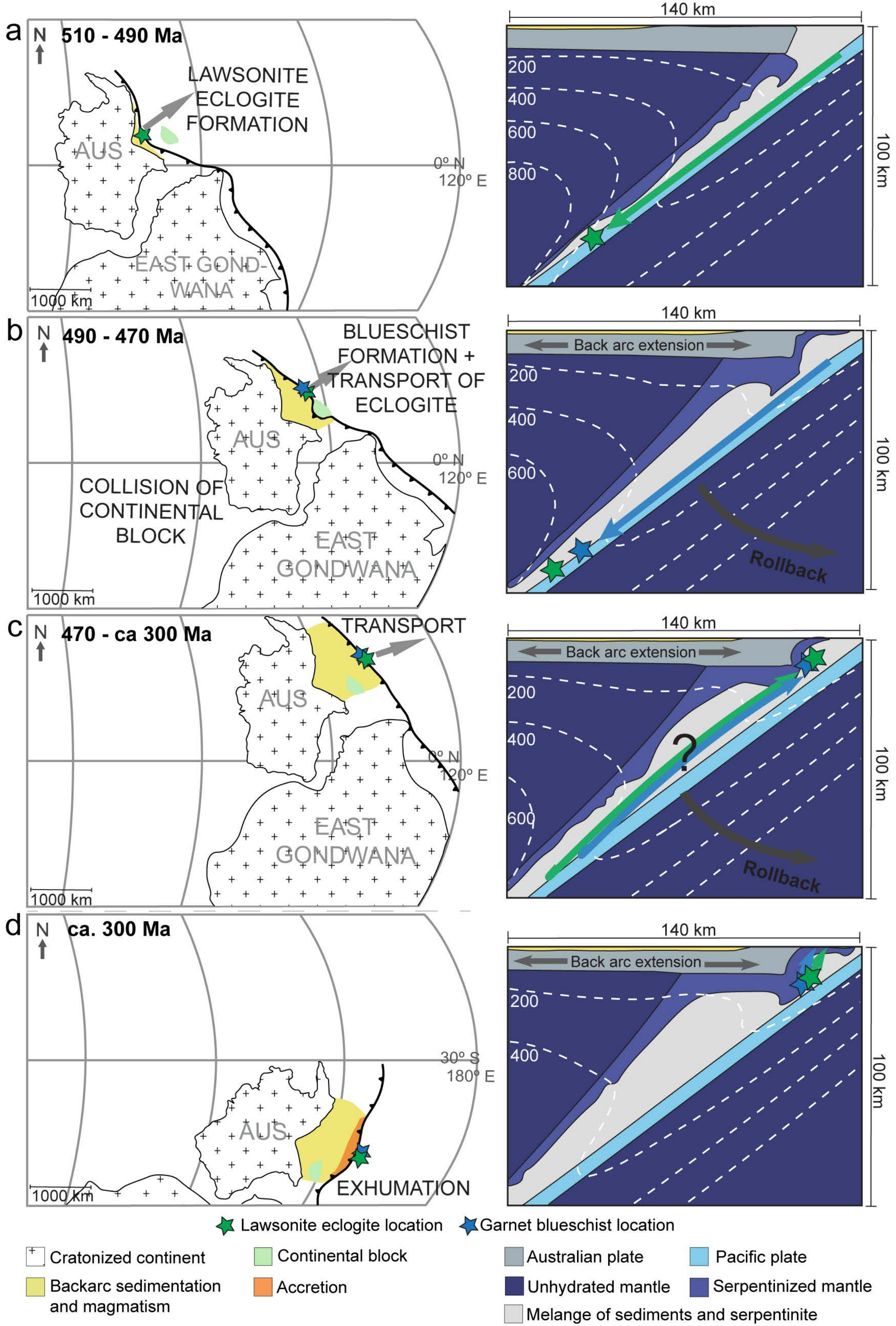
a
N
510 - 490 Ma
LAWSONITE
ECLOGITE
FORMATION
AUS
0º N
120º E
EAST GOND-
WANA
1000 km
140 km
200
400
600
800
100 km
b
N
490 - 470 Ma
BLUESCHIST
FORMATION +
TRANSPORT OF
ECLOGITE
AUS
0º N
120º E
COLLISION OF
CONTINENTAL
BLOCK
EAST
GONDWANA
1000 km
140 km
Back arc extension
200
400
600
100 km
Rollback
c
N
470 - ca 300 Ma
TRANSPORT
AUS
0º N
120º E
EAST
GONDWANA
1000 km
140 km
Back arc extension
200
400
600
?
100 km
Rollback
d
N
ca. 300 Ma
30º S
180º E
AUS
EXHUMATION
1000 km
140 km
Back arc extension
200
400
100 km
Lawsonite eclogite location
Garnet blueschist location
Cratonized continent
Continental block
Australian plate
Pacific plate
Backarc sedimentation and magmatism
Accretion
Unhydrated mantle
Serpentinized mantle
Melange of sediments and serpentinite